THE JOURNAL OF BIOLOGICAL CHEMISTRY VOL. 286, NO. 35, pp. 30837–30846, September 2, 2011

Phosphoinositide 3-Kinase (PI3K(p110α)) Directly Regulates Key Components of the Z-disc and Cardiac Structure*[S]

Received for publication, June 13, 2011, and in revised form, July 7, 2011 Published, JBC Papers in Press, July 11, 2011, DOI 10.1074/jbc.M111.271684

Ashley J. Waardenberg[‡§], Bianca C. Bernardo[¶], Dominic C. H. Ng[‖], Peter R. Shepherd[‡‡], Nelly Cemerlang[¶], Mauro Sbroggiò[§§], Christine A. Wells[‡¶¶], Brian P. Dalrymple[§], Mara Brancaccio[§§], Ruby C. Y. Lin[‖‖1], and Julie R. McMullen[¶1,2]**

From the [‡]Eskitis Institute for Cell and Molecular Therapies, Griffith University, Nathan, Queensland, 4111, Australia, [§]Commonwealth Scientific and Industrial Research Organisation, Food Futures Flagship, Queensland Bioscience Precinct, St. Lucia, Queensland, 4067, Australia, the [¶]Baker IDI Heart and Diabetes Institute, Melbourne, Victoria, 8008, Australia, the [‖]Department of Biochemistry and Molecular Biology, Bio21 Institute, University of Melbourne, Melbourne, Victoria, 3010, Australia, the [**]Department of Molecular Medicine, University of Auckland, Grafton, Auckland, 1142, New Zealand, the [‡‡]Maurice Wilkins Centre for Molecular Biodiscovery, University of Auckland, Grafton, Auckland, 1142, New Zealand, the [§§]Department of Genetics, Biology, and Biochemistry, University of Torino, Molecular Biotechnology Center, Torino, 10126, Italy, the [¶¶]Australian Institute for Bioengineering and Nanotechnology, The University of Queensland, Brisbane, Queensland, 4072, Australia, and the [‖‖]Ramaciotti Centre for Gene Function Analysis and the School of Biotechnology and Biomolecular Sciences, University of New South Wales, Sydney, New South Wales, 2052, Australia

Maintenance of cardiac structure and Z-disc signaling are key factors responsible for protecting the heart in a setting of stress, but how these processes are regulated is not well defined. We recently demonstrated that PI3K(p110α) protects the heart against myocardial infarction. The aim of this study was to determine whether PI3K(p110α) directly regulates components of the Z-disc and cardiac structure. To address this question, a unique three-dimensional virtual muscle model was applied to gene expression data from transgenic mice with increased or decreased PI3K(p110α) activity under basal conditions (sham) and in a setting of myocardial infarction to display the location of structural proteins. Key findings from this analysis were then validated experimentally. The three-dimensional virtual muscle model visually highlighted reciprocally regulated transcripts associated with PI3K activation that encoded key components of the Z-disc and costamere, including melusin. Studies were performed to assess whether PI3K and melusin interact in the heart. Here, we identify a novel melusin-PI3K interaction that generates lipid kinase activity. The direct impact of PI3K(p110α) on myocyte structure was assessed by treating neonatal rat ventricular myocytes with PI3K(p110α) inhibitors and examining the myofiber morphology of hearts from PI3K transgenic mice. Results demonstrate that PI3K is critical for myofiber maturation and Z-disc alignment. In summary, PI3K regulates the expression of genes essential for cardiac structure and Z-disc signaling, interacts with melusin, and is critical for Z-disc alignment.

An important question in cardiac biology is what makes one heart stronger, or more capable of resisting stress, than another. Maintenance of cardiac structure and Z-disc signaling are considered key factors responsible for protecting the heart in a setting of stress. Mutations of genes encoding proteins of the costamere and Z-disc have been linked with cardiomyopathies in animals and humans (1, 2). Costameres are specialized membrane junctions that physically connect the Z-disc to the basal lamina outside of the cell. The Z-disc is well recognized for its role in maintaining structural integrity and, more recently, has emerged as a "hot spot" or nodal hub of cardiomyocyte signaling, converting mechanical signals into chemical signals, leading to a transcriptional response and induction of a cardiac phenotype such as hypertrophy (1). Despite progress in this area, the mechanisms responsible for regulating components of the costamere and Z-disc are not well defined (2).

The p110α isoform of phosphoinositide 3-kinase (PI3K(p110α)/PIK3CA) has cardioprotective properties (3). We recently demonstrated that cardiac expression of a constitutively active (ca)[3] PI3K transgene (increased PI3K activity) provided protection in a mouse model of myocardial infarction (MI), whereas a reduction in cardiac PI3K activity (utilizing a dominant negative (dn) PI3K transgene) accelerated the progression of heart failure (4). This makes targeting the PI3K pathway an attractive approach for developing new treatment strategies for heart failure.

* This work was supported by postgraduate scholarships from Griffith University and the Commonwealth Scientific and Industrial Research Organisation Food Futures National Research Flagship (to A. J. W.) and by National Health and Medical Research Council (NHMRC) Project Grant 367600 (to J. R. M.). This work was supported in part by the Victorian Government Operational Infrastructure Support Program. This work was also supported by Australian Research Council Future Fellowship FT0001657 (to J. R. M.), Honorary NHMRC Senior Research Fellowship 586604 (to J. R. M.), NHMRC Peter Doherty Fellowship 351012 (to R. C. Y. L.), University of New South Wales Vice Chancellor Research Fellowship (to R. C. Y. L.), and by an University of Melbourne Roper fellowship (to D. C. H. N.).

[S] The on-line version of this article (available at http://www.jbc.org) contains supplemental Tables I–III and additional methods, equations, and references.

[1] Both authors contributed equally to this work.

[2] To whom correspondence should be addressed: Baker IDI Heart and Diabetes Institute, Melbourne, Victoria, 8008, Australia. Tel.: 61-3-85321194; Fax: 61-3-85321100; E-mail: julie.mcmullen@bakeridi.edu.au.

[3] The abbreviations used are: ca, constitutionally active; MI, myocardial infarction; dn, dominant negative; IGF1, insulin-like growth factor 1; VMus3D, three-dimensional virtual muscle model; Ntg, non-transgenic; NRVM, neonatal rat ventricular myocyte(s).

PI3K(p110α) is a key mediator of insulin-like growth factor 1 (IGF1)-induced and exercise-induced beneficial physiological cardiac hypertrophy (5). Unlike pathological hypertrophy/enlargement, physiological cardiac hypertrophy is not an independent predictor of cardiovascular mortality and has protective properties (3). IGF1 administered directly onto neonatal cardiomyocytes *in vitro* increased mRNA expression and translation of contractile proteins, implicating a possible link between activation of the IGF1-PI3K axis and regulation of the expression of cardiac muscle structural components (6).

The primary aim of this study was to determine whether PI3K(p110α) specifically regulates cardiac structural components. We hypothesized that regulation of cardiac structure by PI3K(p110α) may explain why caPI3K hearts are protected against a cardiac insult, whereas dnPI3K hearts are more susceptible to heart failure. To address this question, we subjected microarray data from PI3K transgenic mice under basal conditions (sham) and in a setting of MI (4) to a recently developed tool for visualizing changes in gene expression spatially across a three-dimensional virtual muscle model (VMus3D) (7). The VMus3D tool is a simple, fast approach that highlights differential expression of genes related to muscle structure, identifying regulatory/structural relationships otherwise hidden from more generalist mining approaches. Key findings from this analysis were then validated experimentally.

EXPERIMENTAL PROCEDURES

Experimental Design—The VMus3D model (described below) was applied to previously reported gene expression data (4) (GEO accession number GSE 7487) from cardiac-specific transgenic mouse models with increased or decreased PI3K activity under basal conditions (sham) and in response to MI. The experimental design encompassed a comparison of six models that lie on a spectrum ranging from a physiological "protective" model (*i.e.* caPI3K sham) to an accelerated heart failure phenotype (*i.e.* dnPI3K MI). Such a design optimizes the ability to accurately link molecular signatures with specific phenotypes.

The molecular phenotypes of the six groups are as follows: 1) Non-transgenic (Ntg/control, FVB/N background) sham: Normal cardiac function and gene signature. 2) dnPI3K sham: Normal cardiac function at baseline, gene signature reflecting a heart susceptible to stress. 3) caPI3K sham: Normal cardiac function at baseline, physiological gene signature reflecting a heart protected against stress. 4) Ntg MI: Poor cardiac function, heart failure/pathological gene signature. 5) dnPI3K MI: Very poor cardiac function, gene signature reflecting accelerated heart failure in comparison to Ntg MI. 6) caPI3K MI: Better cardiac function than Ntg MI, a gene signature reflecting a slowing of the heart failure process compared with Ntg MI.

VMus3D Modeling—Affymetrix probe set data generated were normalized using the robust multiarray average method (8, 9), then entered into VMus3D for visualizing gene expression changes in terms of location of their protein product in muscle structure (further details are presented in the supplemental material and Ref. 7). Visualization was limited to genes with p values ≤ 0.05 and colored using VMus3D according to their significance and the direction of fold change being positive or negative. A two-by-two contingency table was constructed to compare reciprocally expressed genes observed using VMus3D in sham and infarct settings. Significance was assessed using the Barnard test and performed in R (10, 11).[4]

Gene lists were selected on the basis of the patterns recognized using VMus3D, as described by criteria presented in the supplemental material. The resulting lists were subjected to gene set enrichment via DAVID (12).

Protein Analysis and Kinase Activity Assays—Heart lysates were prepared as described (4). Western blot analysis: For IGF1R, blots were probed with an anti-IGF1R β (Santa Cruz Biotechnology, Inc., sc-713, 1:1000) followed by an anti-GAPDH (Santa Cruz Biotechnology, Inc., sc-32233,1:5000). For Akt and ERK1/2, blots were probed with phospho-(Ser-473)Akt (#9271), Akt (#9272), phospho-ERK1/2 (#9101) and ERK1/2 (#9102) (all from Cell Signaling Technology, Inc.).

IRS1 Immunoprecipitation—Immunoprecipitation was performed as described previously (13) using 1.5 mg of heart lysate, protein A-Sepharose, and an anti-IRS1 antibody (Millipore, #06–248, 0.25 mg/ml). Blots were probed with the anti-IRS1 antibody (1:2000).

PI3K Activity/Lipid Kinase Activity—PI3K activity was assessed in mouse ventricular tissue (13, 14). Heart tissue lysate (1 mg) was immunoprecipitated with an anti-p85 antibody (0.5 μl, Millipore, #06–195) or an anti-melusin antibody (5 μg) (15) and subjected to an *in vitro* lipid kinase assay using phosphatidylinositol as a substrate. Part of the immunoprecipitated enzyme was subjected to Western blotting and probed with the anti-p85 antibody (1:5000) and anti-melusin antibody (1 μg/ml).

Interaction between the regulatory subunit of PI3K (p85) and melusin—Heart lysate (5 mg) from wild-type, melusin-null (16), and melusin-overexpressing mice (17) was immunoprecipitated with an anti-melusin antibody (15 μg) (15) followed by an immunoblot with an anti-p85 antibody (1:1000, Cell Signaling Technology, Inc., #4257) and anti-melusin antibody (0.1 μg/ml).

Cell Culture—Neonatal rat ventricular myocyte (NRVM) culture was performed as reported previously (18) and approved by an Institutional Animal Ethics Committee that conforms with the National Institutes of Health Guide for the Care and Use of Laboratory Animals. NRVM were treated with two PI3K(p110α) inhibitors (PIK75 (19) 0–100 μM or A66 (20, 21) 0–50 μM, both from Symansis, Auckland, New Zealand) with and without IGF1 (10 nM, Novozymes Biopharma AU Limited, CM001) for 18 h. Following experimental treatments, cells were either collected for protein lysate isolation and immunoblotting (18) or plated on laminin-coated glass coverslips and fixed in 4% paraformaldehyde for subsequent analysis by immunofluorescence confocal microscopy (18).

Immunofluorescence Confocal Microscopy of NRVM and Heart Sections—NRVM and heart sections (8 μm) from PI3K transgenic mice were analyzed by immunofluorescence staining with antibodies to α-actinin (Sigma-Aldrich), phalloidin (FITC-conjugates, Molecular Probes), DAPI, and Cy2/Cy3-

[4] T. Galili, personal communication.

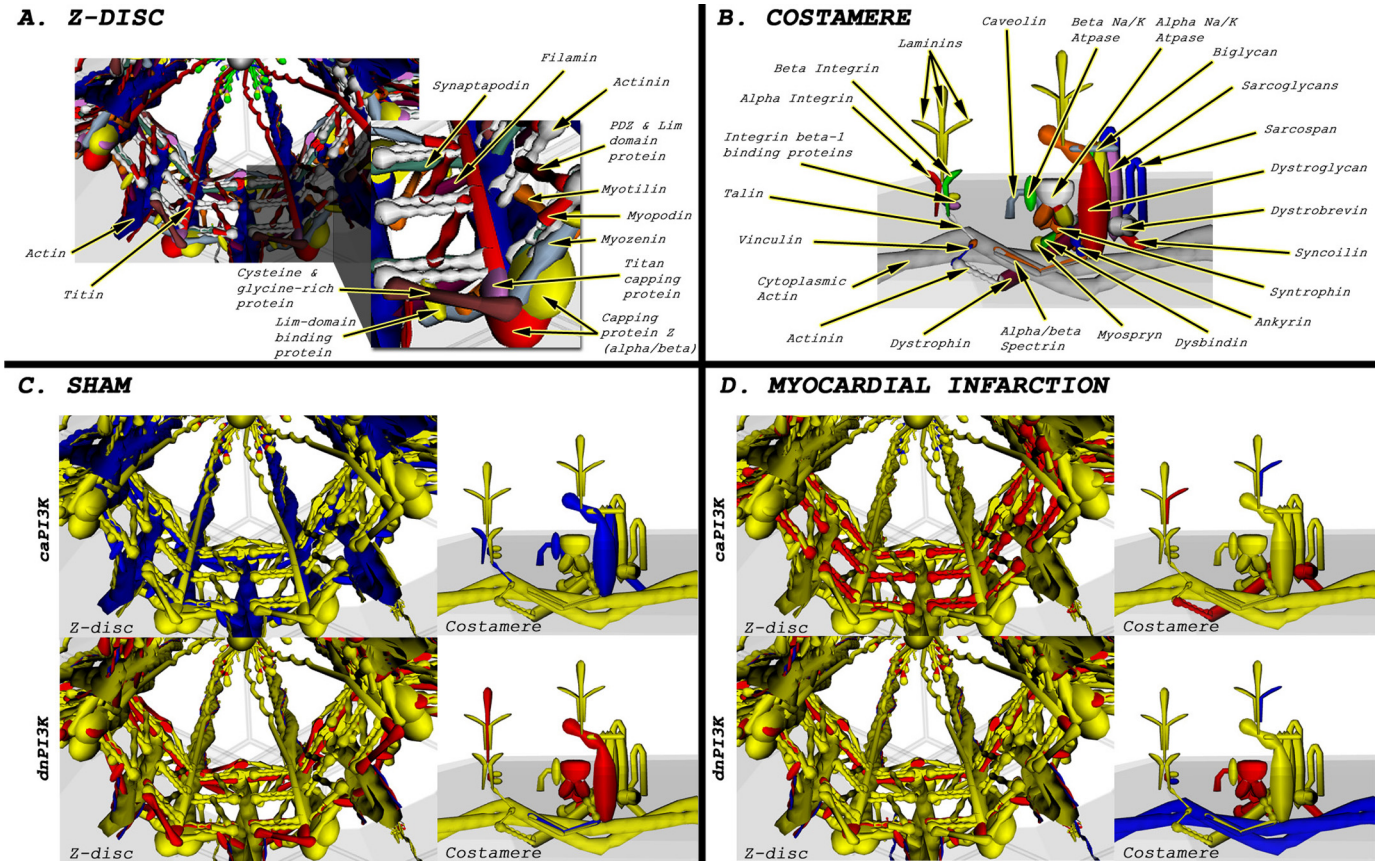

FIGURE 1. **VMus3D visualization of costamere and Z-disc gene expression.** Schematic with labeled components of the Z-disc (*A*) and costamere (*B*). A small section of *A* (highlighted in *gray*) has been enlarged to more readily identify individual components. Gene expression in mice with increased PI3K (caPI3K) and decreased PI3K (dnPI3K) under sham (*C*) and MI conditions (*D*) compared with Ntg. The coloring indicates genes reciprocally expressed ($p < 0.05$) according to PI3K activity in the sham model. *Blue*, positive fold change; *yellow*, no change; *red*, negative fold change.

conjugated secondary antibodies (Chemicon) as described previously (18, 22). Prior to staining, hearts from caPI3K, dnPI3K, and Ntg mice were fixed in HistoChoice® tissue fixative (Amersco) for 4 h at 4 °C and then frozen in Tissue-Tek® O.C.T™ compound (Sakura Finetechnical).

Statistical Analysis—Statistical significance for gene expression data and VMus3D are described under "VMus3D Modeling" and in the supplemental data. Data from protein analysis are presented as mean ± S.E. Significance was determined using one-way analysis of variance ($p < 0.05$) followed by the Fisher's protected least significance post hoc test ($p < 0.05$).

RESULTS

VMus3D Highlighted PI3K(p110α)-regulated Transcripts Encoding Key Components of the Costamere and Z-disc—We reported previously that dnPI3K mice (cardiac PI3K activity decreased by 77%) and caPI3K mice (cardiac PI3K activity increased 6.5-fold) displayed normal cardiac function under sham conditions but displayed distinct phenotypes in response to MI for 8 weeks (4). In a setting of MI, caPI3K mice were protected with better cardiac function than Ntg mice, whereas dnPI3K mice were more susceptible to heart failure progression with poorer cardiac function than Ntg mice (4). VMus3D was used to overlay gene expression data onto structural components of cardiac muscle using data mined from Ntg and PI3K transgenic mice under sham and MI settings (4) (Fig. 1). This highlighted a distinct reciprocal pattern of gene expression between the PI3K transgenic models under sham conditions (Fig. 1*C*, *blue*, up-regulation in caPI3K; *red*, down-regulation in dnPI3K; $p < 0.05$), suggesting that PI3K activity can regulate components of the costamere and Z-disc under basal conditions. This was consistent with the hypothesis that PI3K activity predisposes how the heart will respond to a subsequent cardiac insult such as MI and prompted us to perform a reciprocal expression analysis (dnPI3K *versus* caPI3K) across the full microarray dataset.

Genes encoding muscle structural/associated proteins that were differentially and reciprocally expressed in the PI3K models under sham conditions included dystroglycan (Dag1), filamin C (Flnc), ankyrin repeat domain 23 (Ankrd23/Darp), Rho-associated coiled-coil containing protein kinase 2 (Rock2), crystallin, α B (Cryab), Cd151, integrin β 1 binding protein 2 (Itgb1bp2/melusin), Lim domain binding 3 (Ldb3/cypher), and synaptopodin 2 (Synpo2/myopodin) (supplemental Equations 2 and 3 and Table I, $p \leq 0.05$, Fig. 1). Each of these genes were up-regulated in caPI3K (highlighted in *blue*, Fig. 1) and down-regulated in dnPI3K (highlighted in *red*, Fig. 1) relative to Ntg.

Experimental Evidence for a Novel Interaction between Melusin and PI3K in the Heart—Melusin (Itgb1bp2) is known to interact with the cytoplasmic domain of β1-integrin, is enriched in costameres, and has been shown previously to play

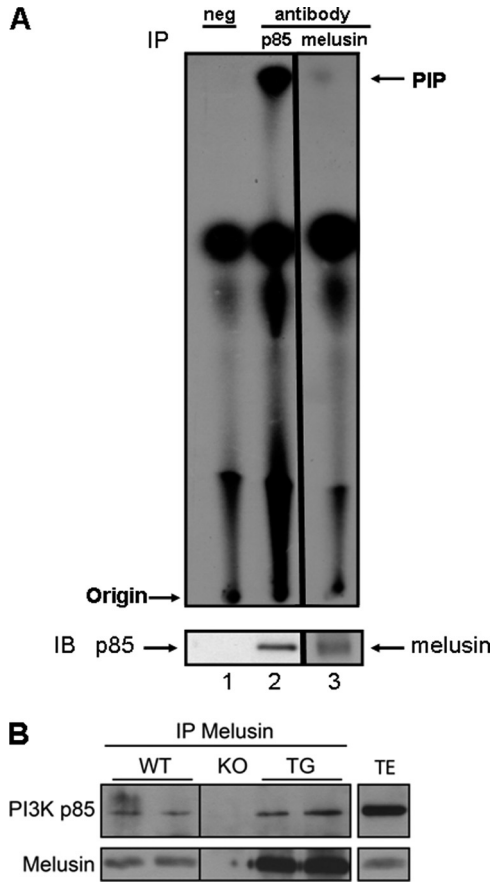

FIGURE 2. **Interaction between PI3K and melusin in the heart.** *A*, heart lysate was immunoprecipitated (*IP*) with anti-p85 antibody (*lane 2*, positive control), anti-melusin antibody (*lane 3*), or no antibody (*lane 1*, negative control) and subjected to a lipid kinase assay using phosphatidyl inositol as a substrate. *PIP*, PtdIns 3-phosphate represents PI3K activity. Part of the immunoprecipitate was subjected to Western blotting (*IB*) and probed with anti-p85 or anti-melusin. *B*, heart lysate from WT, melusin-null (*KO*), and melusin-overexpressing transgenic mice (*TG*) was immunoprecipitated with anti-melusin antibody followed by immunoblotting with anti-p85 and anti-melusin. Heart total extract (*TE*) was run as a reference for the molecular weight of p85. Results were confirmed in four independent experiments.

a critical role in sensing mechanical stress (16). The tail domain of melusin is responsible for the interaction with β1-integrin, whereas the amino-terminal portion of melusin has multiple proline-rich motifs and tyrosine phosphorylation sites that could bind to SH3- and SH2-containing proteins (23). Class IA PI3Ks (including the p110α catalytic subunit) interact with adaptor subunits containing SH2 domains, and the regulatory subunit (85-kDa adaptor) contains an SH3 domain (24), suggesting the possibility of an interaction between PI3K and melusin. To assess whether PI3K and melusin interact in the heart and the potential significance of such a complex, heart tissue lysate was immunoprecipitated with an anti-melusin antibody followed by an *in vitro* lipid kinase assay using PtdIns as a substrate. Lipid kinase activity was observed in the heart lysate immunoprecipitated with the anti-melusin or anti-p85 antibody (positive control) but not the negative control (Fig. 2*A*). To further validate an interaction between melusin and PI3K in the heart, experiments in hearts from wild-type, melusin-null, and melusin-overexpressing mice were performed. Melusin-overexpressing mice allow melusin interactors to be more readily identified, whereas the melusin-null mouse is an ideal control for specificity. In the current study, the p85 regulatory subunit of PI3K was clearly detected in a melusin immunoprecipitate obtained from melusin-overexpressing transgenic mouse heart extracts (*TG*), and a weaker signal for p85 was present in WT heart lysates. In contrast, no signal for p85 was detected in heart lysates from melusin-null mice (*KO*, Fig. 2*B*).

Enrichment of Genes Related to the IGF1 Pathway—To gain further insight as to how PI3K might sense biomechanical stress and regulate muscle structure and Z-disc signaling, we performed a gene set enrichment analysis to investigate the global effects of PI3K perturbation (supplemental Equation 3 and Table II). Analysis against all "pathways" listed in DAVID identified the following pathways ($p < 0.05$): Ribosome (KEGG 0310), IGF1R signaling (BIOCARTA), focal adhesion (KEGG 04510), insulin signaling (KEGG 04910), IGF1 signaling (BIOCARTA), IL-2 receptor β chain in T cell activation (BIOCARTA), and glycerophospholipid metabolism (KEGG 00564). Enrichment of the IGF1-related pathways was of particular interest, given that IGF1 plays an important role in mediating cardiac protection (5), and PI3K(p110α) is a critical downstream mediator of IGF1R-induced physiological heart growth (13).

By microarray, IGF1R and IRS1 mRNA expression were elevated in hearts of Ntg in a setting of MI compared with sham (Fig. 3*A*). IGF1R and IRS1 mRNA expression were lower in caPI3K sham hearts and higher in dnPI3K sham hearts (Fig. 3*A*). IGF1R mRNA expression did not significantly increase in caPI3K or dnPI3K mice in response to MI. To validate that changes at the level of gene expression reflected protein levels, we assessed IGF1R and IRS1 by Western blotting and immunoprecipitation, respectively. Consistent with our gene expression data, we observed parallel changes in protein expression of IGF1R and IRS1 in the sham and MI models (Fig. 3, *B* and *C*).

Direct Evidence of an Impact of PI3K on Cardiac Myocyte Structure—The VMus3D model and subsequent gene set enrichment analysis suggested that IGF1-PI3K(p110α) signaling directly regulates cardiac myocyte structure. To test this hypothesis, we performed two studies. 1) We assessed the impact of two PI3K inhibitors on the myofiber structure in NRVM and 2) examined the myofiber morphology of hearts from Ntg, caPI3K, and dnPI3K under basal conditions.

1) Inhibition of PI3K(p110α) prevents normal formation of mature myofibers under basal conditions and in response to IGF1: NRVM were treated independently with two PI3K(p110α) inhibitors (PIK75 and A66) in the presence or absence of IGF1. PIK75 has been used previously to study the role of PI3K(p110α) but has some off-target activity (19, 25). A66 is considered a more highly specific and selective inhibitor for p110α (20, 21). The specificity of both inhibitors at different doses (0.1–100 μM) was tested in NRVM with or without IGF1. The ratio of pAkt/total Akt was reduced by more than 50% in IGF1 stimulated NRVM with 0.1 μM PIK75 or 0.5 μM A66 and was abolished completely in IGF1-stimulated NRVM treated with 1 μM PIK75 or 10 μM A66 (Fig. 4, *A* and *B*). The PI3K(p110α) inhibitors had no significant impact on pERK/total ERK at these concentrations (Fig. 4, *A* and *B*). At substantially higher concentrations of PIK75 (10 and 100 μM), an increase in ERK phosphorylation stimulated by IGF1 was not

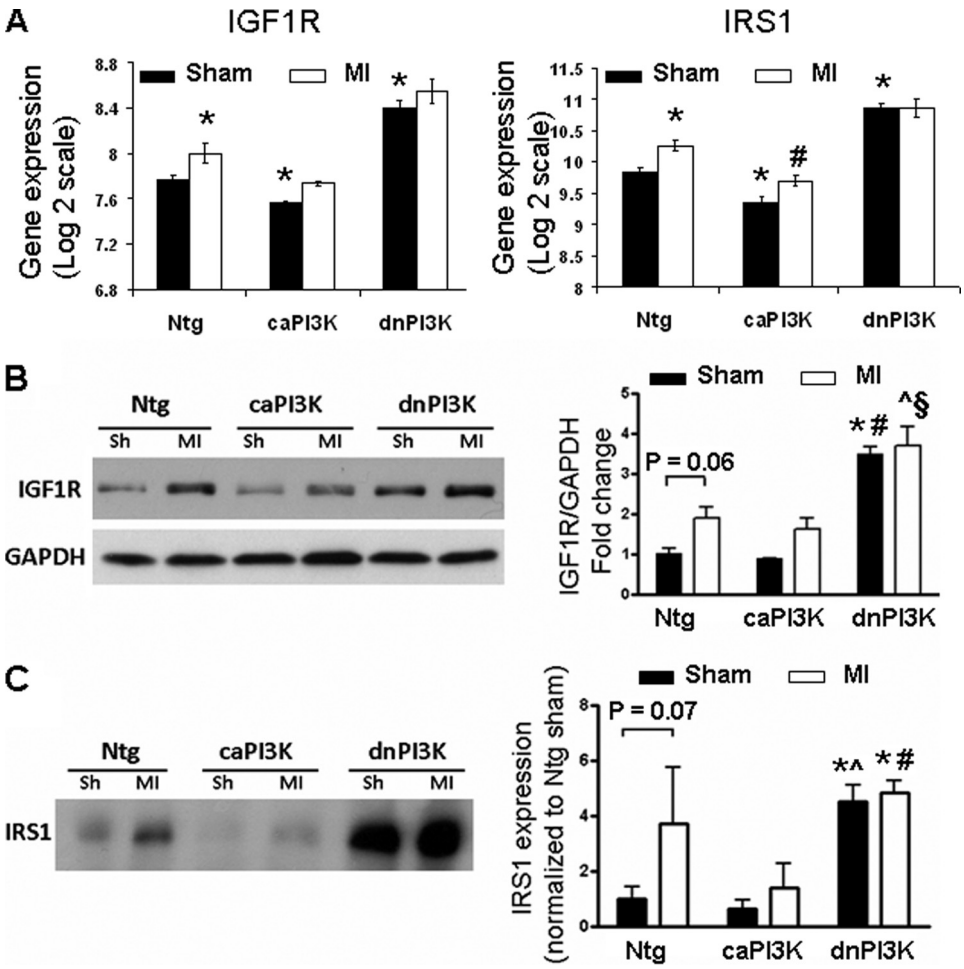

FIGURE 3. **IGF1R and IRS1 gene and protein expression.** *A*, IGF1R and IRS1 gene expression (log2) obtained by microarray. *, $p < 0.05$ *versus* Ntg sham; #, $p < 0.05$ *versus* caPI3K sham. *B*, *left panel*, Western blot analysis of IGF1R and GAPDH in hearts from Ntg, caPI3K, and dnPI3K mice subjected to sham (*Sh*) or MI. *Right panel*, quantitative analysis of IGF1R relative to GAPDH. Mean values for Ntg Sh were normalized to 1. $n = 3$ for Sh groups, $n = 4$ for MI groups. *, $p < 0.0001$ *versus* Ntg Sh and caPI3K Sh; ^, $p < 0.001$ *versus* Ntg MI; §, $p < 0.001$ *versus* caPI3K MI; #, $p < 0.01$ *versus* Ntg MI and caPI3K MI. *C*, *left panel*, immunoprecipitated IRS1. *Right panel*, quantitative analysis of IRS1. Mean values for Ntg were normalized to 1. $n = 3$ for each group. *, $p < 0.05$ *versus* Ntg Sh; ^, $p < 0.05$ *versus* caPI3K Sh; #, $p < 0.05$ *versus* caPI3K MI.

observed (Fig. 4*A*). A66 had no effect on pERK/total ERK, even at 50 μM (Fig. 4*B*).

Myofiber formation and sarcomere organization was examined by immunofluorescence. α-actinin was used to highlight the sarcomeric bands and Z-discs, and phalloidin was used to stain the contractile actin thin filaments. Sarcomeres in the control myocytes ran in multiple axes within the same cell and were generally punctate and non-striated (Fig. 4, *C* and *D*, dimethyl sulfoxide (*DMSO*)). Control cells also had an irregular rounded morphology. In contrast, myocytes treated with the PI3K(p110α) inhibitors alone had an elongated stellate morphology, and sarcomeres tended to run along a longitudinal axis rather than multiple axes (Fig. 4, *C* and *D*, *b* and *c*, *h* and *i*, and *t* and *u*). IGF1 stimulation resulted in an increase in NRVM size, and this was associated with the formation of mature myofibers (increase in the organization of actin myofibrils as assessed by phalloidin staining, with striated sarcomeres running in multiple axes; Fig. 4, *C* and *D*, *d*, *j*, and *v*). The PI3K(p110α) inhibitors prevented the formation of mature myofibers in response to IGF1 stimulation (Fig. 4, *C* and *D*, *e*, *k*, *w*, *f*, *l*, and *x*). Further, A66 at 10 μM was associated with a reduction in phalloidin staining under basal conditions and in the presence of IGF1 (Fig. 4*D*, *i* and *l*).

2) Reduced Z-disc alignment in dnPI3K hearts: Myofiber morphology was assessed in heart sections from adult Ntg, dnPI3K, and caPI3K by immunofluorescence. There were greater numbers of myofilaments and thicker myofibrils in caPI3K hearts compared with Ntg hearts (Fig. 5). In contrast, there were fewer myofilaments and thinner myofibrils in dnPI3K hearts compared with Ntg hearts (Fig. 5). Z-disc alignment (α-actinin stain) appeared reduced in dnPI3K hearts (Fig. 5). Phalloidin staining intensity of actin was markedly reduced in sections from dnPI3K heart (Fig. 5) and is consistent with a reduction in phalloidin staining observed in NRVM treated with A66 (Fig. 4*D*).

DISCUSSION

The development of cardiomyopathy in humans and mouse models with mutations/defects in Z-disc proteins highlight the need to understand the molecular mechanisms that regulate Z-disc biology (2). A greater knowledge of the basic mechanisms responsible will be important for the development of

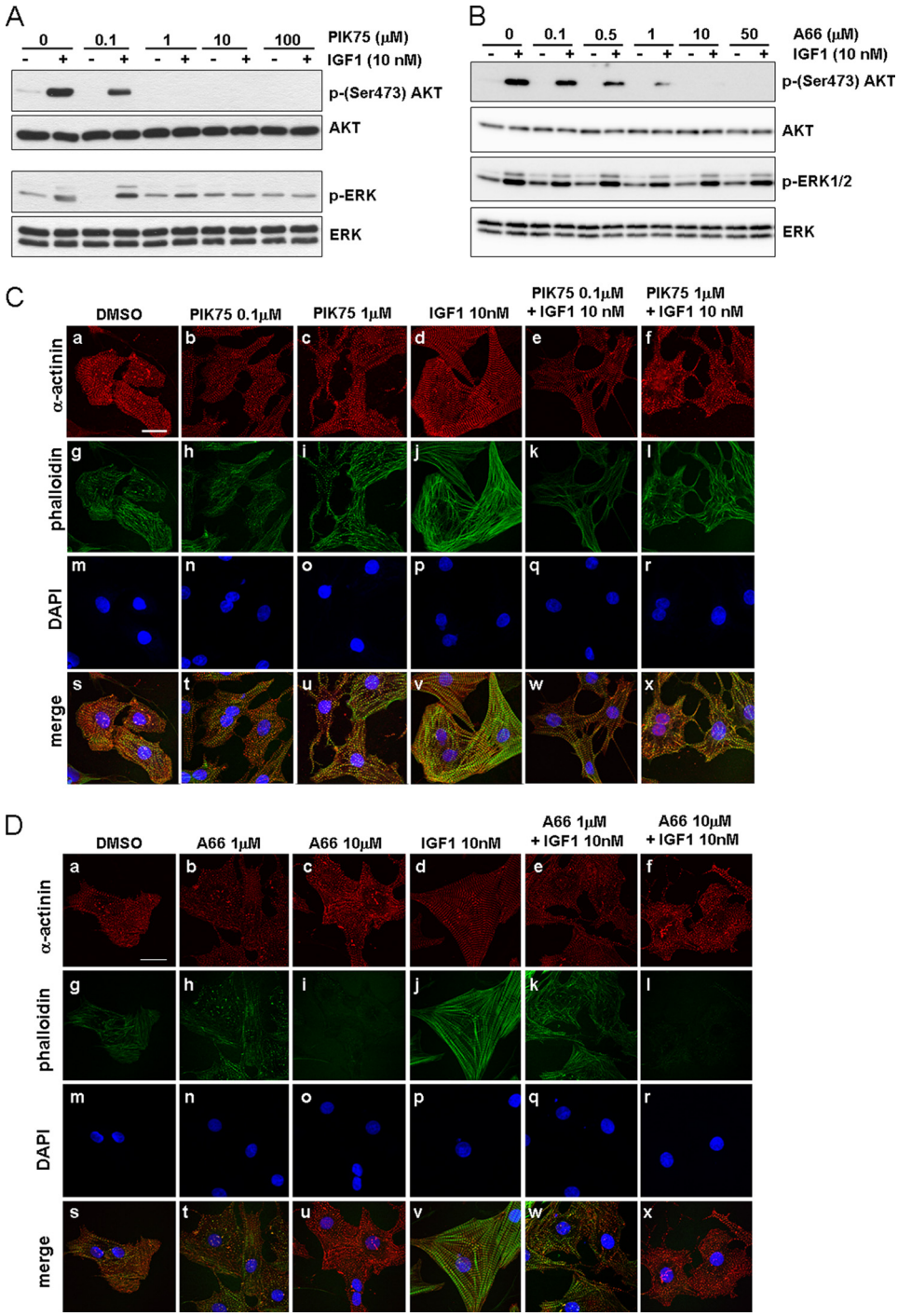

FIGURE 4. **NRVM treated with PI3K(p110α) inhibitors (PIK75 or A66) in the absence and presence of IGF1.** *A* and *B*, Western blot analyses of pAkt, total Akt, pERK, and ERK in cell lysates from NRVM treated with or without IGF1 in the presence of PIK75 (0–100 μm) or A66 (0–50 μm). *C* and *D*, immunofluorescence of control NRVM (dimethyl sulfoxide, *DMSO*) and NRVM treated with PIK75, A66, and/or IGF1 for 18 h. Anti-α actinin (*a–f*) stains sarcomeric bands and Z-lines, phalloidin-FITC (*g–l*) stains contractile thin filaments, and DAPI (*m–r*) stains nuclei. *s–x*, merged images. *Scale bar* = 20 μm. Experiments were repeated twice with identical findings. Representative images from a single experiment are shown.

improved therapeutic strategies for the heart. Z-disc proteins share "sticky" domains that are capable of mediating multiple protein-protein interactions and play an essential role in integrating structure and signaling in the complex three-dimensional network (2). Phosphatases and kinases, including calcineurin and protein kinase C, have been shown previously to reside at the Z-disc (2). However, whether PI3K(p110α) directly regulated cardiac structure and components of the Z-disc was unknown. The goal of this study was to examine whether PI3K(p110α) regulates structural components of cardiac muscle to protect the heart. We demonstrated previously that mice with increased PI3K activity (caPI3K) develop physiological cardiac hypertrophy, whereas mice with decreased PI3K activity have smaller hearts (14, 26). Cardiac function was normal in both models under basal/sham conditions, but under settings of stress (*e.g.* pressure overload, dilated cardiomyopathy, or

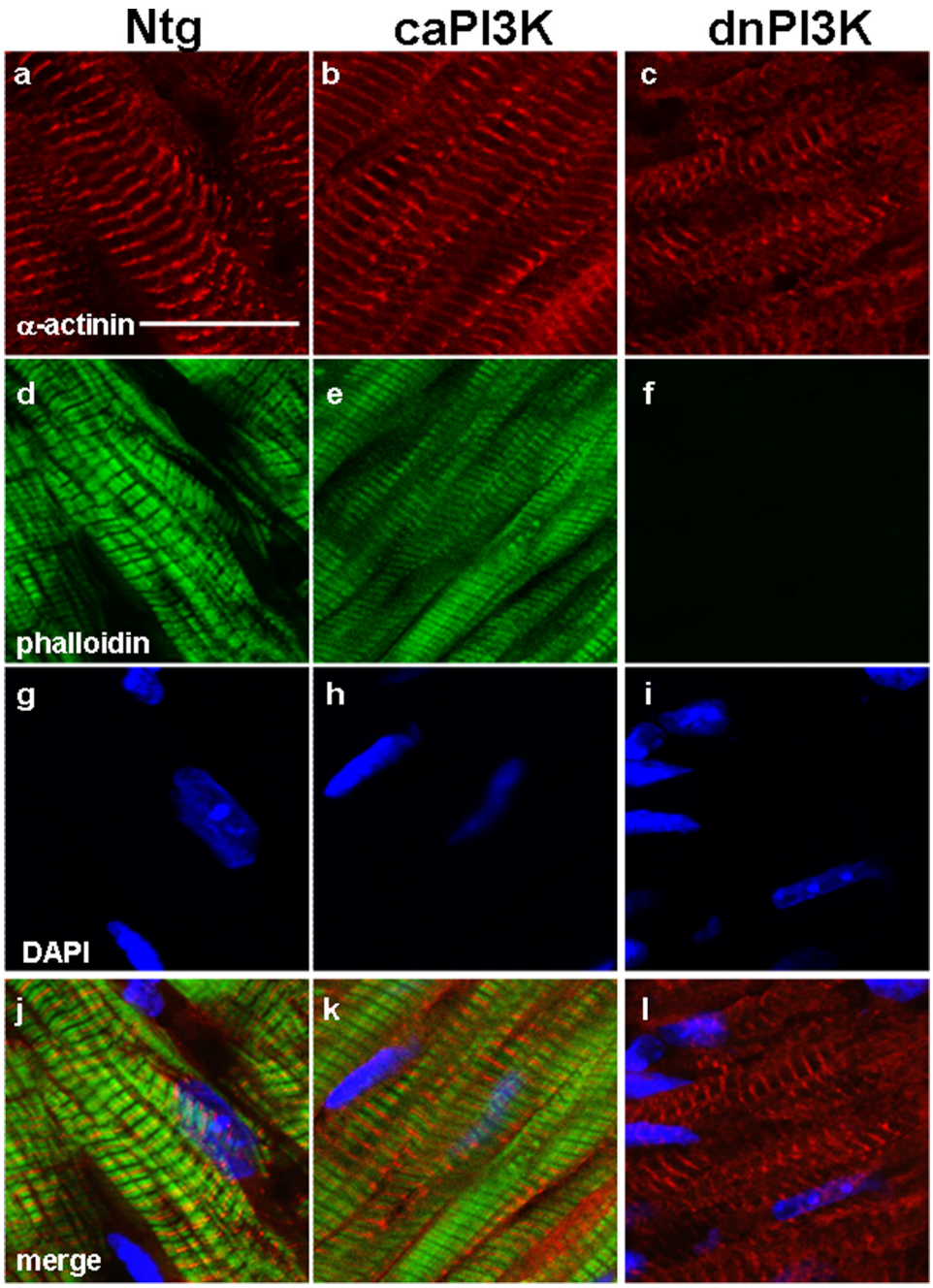

FIGURE 5. **Z-band alignment in myocytes from PI3K transgenic mice.** Representative cross sections from ventricles of Ntg, caPI3K, and dnPI3K mice. Anti-αactinin (*a–c*) stains sarcomeric bands and Z-lines, phalloidin-FITC (*d–f*) stains contractile thin filaments, and DAPI (*g–i*) stains nuclei. *j–l*, merged images. *Scale bar* = 20 μm. $n = 4$ in each group.

MI), caPI3K mice were protected compared with Ntg, whereas dnPI3K mice developed heart failure more rapidly (4, 26–28). We hypothesized that applying the VMus3D model to a robust gene data set from well defined models (*i.e.* genetic models with reciprocal regulation of PI3K in control (sham) and stress settings (MI)) might enable us to uncover reciprocal expression profiles of key elements of the Z-disc that predispose how the heart responds to a subsequent cardiac insult such as MI.

Functional Consequences of Changes in PI3K-regulated Transcripts Encoding Costamere and Z-disc Proteins—Under basal/sham conditions, genes encoding muscle structural/associated proteins that were up-regulated in hearts of caPI3K mice and down-regulated in hearts of dnPI3K mice included dystroglycan (Dag1), filamin C (Flnc), ankyrin repeat domain 23 (Ankrd23/Darp), Rock2, crystallin α B, Cd151, melusin, cypher, and synaptopodin 2 (Synpo2, Myopodin) (Fig. 6). Thus, here we have observed a super-response of muscle structural/mechanosensors in mice with increased activity of PI3K(p110α) *i.e.* caPI3K. There is compelling evidence to demonstrate that altered expression of many of these genes would have a significant impact on functionality of the Z-disc and, subsequently, cardiac function. Dag1 links dystrophin to the extracellular matrix. Cardiomyocyte-specific deletion of Dag1 in mice led to dilated cardiomyopathy that was associated with depressed car-

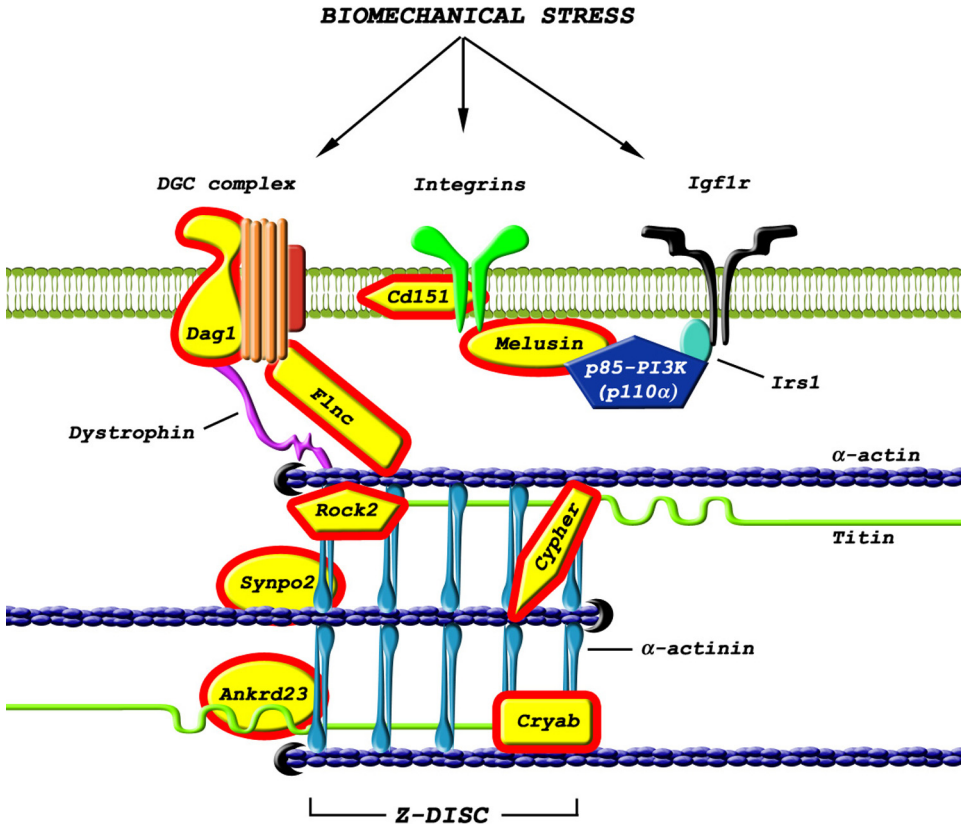

FIGURE 6. **PI3K-regulated components of the costamere and Z-disc.** Model highlighting components of the costamere and Z-disc that are regulated by PI3K. Expression of genes that were up-regulated in caPI3K hearts and down-regulated in dnPI3K hearts are highlighted in *yellow*. The model also highlights the interaction between PI3K and melusin in the heart.

diac function (29). Flnc is a member of the filamin family, expressed in heart and skeletal muscle (30). Filamins stabilize actin filaments and link them to the cell membrane. Filamin mutations in humans have been associated with muscle dysfunction (30). Furthermore, Flnc was identified as a substrate of PI3K activated Akt in mouse heart (31). Ankrd23 belongs to the muscle ankyrin repeat protein (MARP) family and is a structural/regulatory signaling protein that interacts with titin (32). In skeletal muscle, the muscle ankyrin repeat protein family was shown to be protective against eccentric contraction-induced injury (33), suggesting that it plays an important role in maintaining normal structure and function. Finally, cypher is a cytoskeletal protein localized in the sarcomeric Z-disc that was shown to be essential for cardiac sarcomeric structure/stability. Mice with cardiac-specific deletion of cypher or global cypher knockout mice displayed severe cardiac defects and heart failure (34, 35).

Novel Interaction between PI3K and Melusin in the Adult Heart—The reciprocal regulation of melusin in the caPI3K and dnPI3K transgenic mice was of particular interest because melusin-null (16) and melusin-overexpressing transgenic mice (17) display similar phenotypes as dnPI3K and caPI3K transgenic mice, respectively. Both dnPI3K mice and melusin-null mice displayed normal cardiac structure and function under basal conditions but developed dilated cardiomyopathy in response to pressure overload (16, 26, 27). In contrast, melusin-overexpressing and caPI3K transgenic mice displayed a mild physiological hypertrophic phenotype associated with an increase in myocyte size, Akt phosphorylation, and normal cardiac function (14, 17, 27). Further, both models (melusin-overexpressing and caPI3K transgenics) were protected in a setting of pressure overload (17, 27). Collectively, these similarities prompted us to assess whether PI3K and melusin form a complex together in the heart. To our knowledge, we have shown for the first time that the regulatory subunit of PI3K, *i.e.* p85, directly interacts with melusin in the adult heart and generates lipid kinase activity.

The IGF1-PI3K(p110α) Pathway Is an Essential Regulator of Cardiac Structure—Previous studies have demonstrated that G-protein-coupled receptors, including the angiotensin II type 1 receptor, can sense biomechanical stress and regulate components of the Z-disc (2). It has also been shown that cyclic stretch of NRVM stimulated secretion of IGF1 (36) and that treatment of NRVM with IGF1 increased mRNA expression and translation of contractile proteins (6). It was previously unclear whether the IGF1-PI3K(p110α) axis played a critical role in regulating components of the cardiac Z-disc. In this study, a gene enrichment analysis highlighted overrepresentation of components of the IGF1 pathway. Gene and protein expression levels of IGF1R and IRS1 were increased in hearts of Ntg in a setting of MI compared with sham. Given that the IGF1R pathway plays a critical role in mediating cardiac protection (5), we speculate that IGF1R and IRS1 increase in response to stress (*e.g.* MI) as a mechanism for protecting the heart. IGF1R and IRS1 expression levels were lower in caPI3K sham hearts and higher in dnPI3K sham hearts. Further, any

increases in expression of IGF1R/IRS1 in a setting of MI were smaller or absent in the PI3K transgenic mice. We hypothesize that in a heart susceptible to stress (*i.e.* dnPI3K sham), the heart attempts to compensate by increasing IGF1R signaling, but because PI3K is a critical effector of the IGF1R pathway, the dnPI3K transgene prevents an increase in structural components and Z-disc signaling that would otherwise provide protection. By contrast, it is not necessary for IGF1R signaling to be elevated in the caPI3K heart because structural components are enhanced already. Our VMus3D model highlighted distinct reciprocal regulation of structural components of the costamere and Z-disc that support this hypothesis, *i.e.* up-regulation in caPI3K and down-regulation in dnPI3K.

To ascertain whether PI3K(p110α) had a direct impact on cardiac structure, we used two independent approaches. First, we examined the impact of two PI3K(p110α) inhibitors on the structure of NRVM under basal conditions and in the presence of IGF1. Second, we examined the structure of cardiac sections from caPI3K and dnPI3K mice in comparison to Ntg. Both studies demonstrated that PI3K(p110α) has an impact on myofiber morphology and is critical for Z-disc alignment. PI3K(p110α) inhibitor-treated NRVM (without stimulation) displayed sarcomeres that typically ran in a longitudinal axis rather than multiple axes. IGF1 treatment was associated with the formation of mature myofibers, which was prevented in the presence of the PI3K(p110α) inhibitors. caPI3K hearts contained greater numbers of myofilaments and thicker myofibrils than Ntg, whereas dnPI3K hearts contained fewer myofilaments and thinner myofibrils. These findings are consistent with the development of physiological hypertrophy in caPI3K transgenic mice and the small heart phenotype of dnPI3K transgenic mice (14). Z-disc alignment was reduced in dnPI3K hearts, and phalloidin staining intensity of actin was markedly reduced in sections from dnPI3K hearts. This finding is consistent with reduced phalloidin staining of actin in NRVM pretreated with A66. Decreased phalloidin staining in dnPI3K mice is considered reflective of dysregulated sarcomere morphology, as opposed to these mice lacking actin filaments in their hearts, because there was no evidence of differentially expressed genes representative of the actin family in dnPI3K hearts. Collectively, the above findings suggest a defect in myofibril formation and Z-disc alignment in myocytes with reduced PI3K activity.

Targeting the PI3K Pathway with Caution: Heart Failure versus Cancer—Manipulating components of the PI3K pathway has been recognized as the most active drug development in the cancer field (37). PI3K is commonly constitutively activated because of a mutation in many cancers (38). Our previous work demonstrated that dnPI3K mice were more susceptible to the development of atrial fibrillation and/or heart failure than control mice when exposed to pathological insults, including pressure overload (26, 27), dilated cardiomyopathy (28), and MI (4). These findings raise potential concerns for the effects of PI3K inhibitors on the hearts of cancer patients. The very distinct effects of PI3K activation on components of the costamere and Z-disc under basal conditions (sham) in this study provide important new insights as to why inhibition of PI3K makes the heart susceptible to a cardiac insult and highlights that caution must be taken when considering the administration of PI3K inhibitors to patients.

In summary, understanding the very complex process of mechanotransduction in cardiomyocytes is of utmost importance to our knowledge of how the heart responds in a setting of stress and will be critical for the development of more effective treatment strategies for heart failure. Here we have used a novel approach to visualize genes expressing proteins that form part of the cardiac contractile apparatus that are regulated by PI3K. To our knowledge, we have shown for the first time that PI3K can directly affect components of the costamere and Z-disc, PI3K complexes with melusin in the heart, and that PI3K has a direct impact on cardiac myofiber maturation and Z-disc alignment. Collectively, our data suggest that activation of PI3K is a key mechanism that enables structural remodeling of the costamere and Z-disc to protect the heart in a setting of stress.

REFERENCES

1. Samarel, A. M. (2005) *Am. J. Physiol. Heart Circ. Physiol.* **289,** H2291–2301
2. Frank, D., and Frey, N. (2011) *J. Biol. Chem.* **286,** 9897–9904
3. Bernardo, B. C., Weeks, K. L., Pretorius, L., and McMullen, J. R. (2010) *Pharmacol. Ther.* **128,** 191–227
4. Lin, R. C., Weeks, K. L., Gao, X. M., Williams, R. B., Bernardo, B. C., Kiriazis, H., Matthews, V. B., Woodcock, E. A., Bouwman, R. D., Mollica, J. P., Speirs, H. J., Dawes, I. W., Daly, R. J., Shioi, T., Izumo, S., Febbraio, M. A., Du, X. J., and McMullen, J. R. (2010) *Arterioscler. Thromb. Vasc. Biol.* **30,** 724–732
5. McMullen, J. R. (2008) *Clin. Exp. Pharmacol. Physiol.* **35,** 349–354
6. Ito, H., Hiroe, M., Hirata, Y., Tsujino, M., Adachi, S., Shichiri, M., Koike, A., Nogami, A., and Marumo, F. (1993) *Circulation* **87,** 1715–1721
7. Waardenberg, A. J., Reverter, A., Wells, C. A., and Dalrymple, B. P. (2008) *BMC Syst. Biol.* **2,** 88
8. Li, C., and Wong, W. H. (2001) *Proc. Natl. Acad. Sci. U.S.A.* **98,** 31–36
9. Nishiyama, A., Kambe, F., Kamiya, K., Seo, H., and Toyama, J. (1998) *Cardiovasc. Res.* **40,** 343–351
10. Barnard, G. A. (1947) *Biometrika* **34,** 123–138
11. Deleted in proof
12. Dennis, G., Jr., Sherman, B. T., Hosack, D. A., Yang, J., Gao, W., Lane, H. C., and Lempicki, R. A. (2003) *Genome Biol.* **4,** P3
13. McMullen, J. R., Shioi, T., Huang, W. Y., Zhang, L., Tarnavski, O., Bisping, E., Schinke, M., Kong, S., Sherwood, M. C., Brown, J., Riggi, L., Kang, P. M., and Izumo, S. (2004) *J. Biol. Chem.* **279,** 4782–4793
14. Shioi, T., Kang, P. M., Douglas, P. S., Hampe, J., Yballe, C. M., Lawitts, J., Cantley, L. C., and Izumo, S. (2000) *EMBO J.* **19,** 2537–2548
15. Sbroggiò, M., Ferretti, R., Percivalle, E., Gutkowska, M., Zylicz, A., Michowski, W., Kuznicki, J., Accornero, F., Pacchioni, B., Lanfranchi, G., Hamm, J., Turco, E., Silengo, L., Tarone, G., and Brancaccio, M. (2008) *FEBS Lett.* **582,** 1788–1794
16. Brancaccio, M., Fratta, L., Notte, A., Hirsch, E., Poulet, R., Guazzone, S., De Acetis, M., Vecchione, C., Marino, G., Altruda, F., Silengo, L., Tarone, G., and Lembo, G. (2003) *Nat. Med.* **9,** 68–75
17. De Acetis, M., Notte, A., Accornero, F., Selvetella, G., Brancaccio, M., Vecchione, C., Sbroggiò, M., Collino, F., Pacchioni, B., Lanfranchi, G., Aretini, A., Ferretti, R., Maffei, A., Altruda, F., Silengo, L., Tarone, G., and Lembo, G. (2005) *Circ. Res.* **96,** 1087–1094
18. Ng, D. C., Ng, I. H., Yeap, Y. Y., Badrian, B., Tsoutsman, T., McMullen, J. R., Semsarian, C., and Bogoyevitch, M. A. (2011) *J. Biol. Chem.* **286,** 1576–1587
19. Knight, Z. A., Gonzalez, B., Feldman, M. E., Zunder, E. R., Goldenberg, D. D., Williams, O., Loewith, R., Stokoe, D., Balla, A., Toth, B., Balla, T., Weiss, W. A., Williams, R. L., and Shokat, K. M. (2006) *Cell* **125,** 733–747
20. Sun, M., Hillmann, P., Hofmann, B. T., Hart, J. R., and Vogt, P. K. (2010) *Proc. Natl. Acad. Sci. U.S.A.* **107,** 15547–15552

21. Jamieson, S. M., Flanagan, J. U., Kolekar, S., Buchanan, C., Kendall, J. A., Lee, W. J., Rewcastle, G. W., Denny, W. A., Singh, R., Dickson, J., Baguley, B., and Shepherd, P. R. (2011) *Biochem. J.* **438,** 53–62
22. Ng, D. C., Gebski, B. L., Grounds, M. D., and Bogoyevitch, M. A. (2008) *Cell Motil. Cytoskeleton* **65,** 40–58
23. Brancaccio, M., Guazzone, S., Menini, N., Sibona, E., Hirsch, E., De Andrea, M., Rocchi, M., Altruda, F., Tarone, G., and Silengo, L. (1999) *J. Biol. Chem.* **274,** 29282–29288
24. Vanhaesebroeck, B., Leevers, S. J., Panayotou, G., and Waterfield, M. D. (1997) *Trends Biochem. Sci.* **22,** 267–272
25. Chaussade, C., Rewcastle, G. W., Kendall, J. D., Denny, W. A., Cho, K., Grønning, L. M., Chong, M. L., Anagnostou, S. H., Jackson, S. P., Daniele, N., and Shepherd, P. R. (2007) *Biochem. J.* **404,** 449–458
26. McMullen, J. R., Shioi, T., Zhang, L., Tarnavski, O., Sherwood, M. C., Kang, P. M., and Izumo, S. (2003) *Proc. Natl. Acad. Sci. U.S.A.* **100,** 12355–12360
27. McMullen, J. R., Amirahmadi, F., Woodcock, E. A., Schinke-Braun, M., Bouwman, R. D., Hewitt, K. A., Mollica, J. P., Zhang, L., Zhang, Y., Shioi, T., Buerger, A., Izumo, S., Jay, P. Y., and Jennings, G. L. (2007) *Proc. Natl. Acad. Sci. U.S.A.* **104,** 612–617
28. Pretorius, L., Du, X. J., Woodcock, E. A., Kiriazis, H., Lin, R. C., Marasco, S., Medcalf, R. L., Ming, Z., Head, G. A., Tan, J. W., Cemerlang, N., Sadoshima, J., Shioi, T., Izumo, S., Lukoshkova, E. V., Dart, A. M., Jennings, G. L., and McMullen, J. R. (2009) *Am. J. Pathol.* **175,** 998–1009
29. Michele, D. E., Kabaeva, Z., Davis, S. L., Weiss, R. M., and Campbell, K. P. (2009) *Circ. Res.* **105,** 984–993
30. Zhou, A. X., Hartwig, J. H., and Akyürek, L. M. (2010) *Trends Cell Biol.* **20,** 113–123
31. Murray, J. T., Campbell, D. G., Peggie, M., Mora, A., Alfonso, M., and Cohen, P. (2004) *Biochem. J.* **384,** 489–494
32. Miller, M. K., Bang, M. L., Witt, C. C., Labeit, D., Trombitas, C., Watanabe, K., Granzier, H., McElhinny, A. S., Gregorio, C. C., and Labeit, S. (2003) *J. Mol. Biol.* **333,** 951–964
33. Barash, I. A., Bang, M. L., Mathew, L., Greaser, M. L., Chen, J., and Lieber, R. L. (2007) *Am. J. Physiol. Cell Physiol.* **293,** C218–227
34. Zheng, M., Cheng, H., Li, X., Zhang, J., Cui, L., Ouyang, K., Han, L., Zhao, T., Gu, Y., Dalton, N. D., Bang, M. L., Peterson, K. L., and Chen, J. (2009) *Hum. Mol. Genet.* **18,** 701–713
35. Zhou, Q., Chu, P. H., Huang, C., Cheng, C. F., Martone, M. E., Knoll, G., Shelton, G. D., Evans, S., and Chen, J. (2001) *J. Cell Biol.* **155,** 605–612
36. Shyu, K. G., Ko, W. H., Yang, W. S., Wang, B. W., and Kuan, P. (2005) *Cardiovasc. Res.* **68,** 405–414
37. Cheng, H., and Force, T. (2010) *Circ. Res.* **106,** 21–34
38. McMullen, J. R., and Jay, P. Y. (2007) *Cell Cycle* **6,** 910–913

Supplemental Data

Data analysis of microarrays

Microarray data was processed using RMA normalization (Partek v6.4, Partek Inc. St. Louis, Missouri). Principle component analysis was used to ensure batch and technical variations were within limits. Differences across genotypes were compared using analysis of variance and unpaired *t*-test to look for differences between specific genotypes. This analysis demonstrated that 3212 genes were differentially expressed at a q value of 0.01. For detecting differentially expressed genes, the multiple-test correction of p-value was performed by using the positive false discovery rate (FDR) and genes were filtered by a given q-value threshold (1). For full details of this analysis, see: (2). Where multiple annotations of probes to the same gene occurred these were filtered by selecting genes with the highest mean expression across all genotypes.

VMus3D model

Construction of the VMus3D model

Construction of VMus3D has previously been described in detail (3). In brief, AC3D version 6 was used to build de-convoluted 3D models of the structural proteins and their arrangements within muscle (4). Data used for the construction of simplified structures was restricted to evidence from vertebrate due to muscle structural similarity and included where possible: protein-protein interaction data from public data repositories (HPRD and BIND), published experimental protein localization data, structural protein data, and previously published diagrammatic representations of the contractile apparatus (5-11).

Selection of gene lists using VMus3D

Gene lists were selected based on the patterns recognised using VMus3D as per the following criteria:

Equation 1: sham only and reciprocal:

Eq1(i): $p(cS \leq 0.05, dS \leq 0.05)$

DE(+cS, -dS) or DE(-cS, +dS)

(ii): $p(cM > 0.05, dM > 0.05)$

DE(+cS, -dS) or DE(-cS, +dS)

Equation 2: all significant and reciprocal:

Eq2: $p(cS \leq 0.05, dS \leq 0.05, cM \leq 0.05, dM \leq 0.05)$

DE(+cS, -dS) or DE(-cS, +dS)

DE(+cM, -dM) or DE(-cM, +dM)

Equation 3: sham or infarct significant:

Eq3: $p(cS \leq 0.05, dS \leq 0.05)$ or $p(cM \leq 0.05, dM \leq 0.05)$

where,

cS = caPI3K sham vs. Ntg sham

dS = dnPI3K sham vs. Ntg sham

cM = caPI3K MI vs. Ntg MI

dM = dnPI3K MI vs. Ntg MI

DE= differentially expressed

A Boolean descriptive index of direction of gene expression across the models was constructed (Supp table III). 183 significant genes were identified as significantly reciprocally differentially expressed in the sham models and 60 genes were identified across all models amongst 973 identified as differentially expressed in either sham (dnPI3K and caPI3K) or MI (dnPI3K and caPI3K) irrespective of direction of expression. Significant differential expression was relative to Ntg mice.

Gene set enrichment analysis

The resulting gene list generated from equation 3 was subject to gene set enrichment via DAVID (12). The gene list was uploaded using the functional annotation tool; identifier used was official gene symbol and list type selected as gene list using *Mus musculus* as background. All pathways listed in DAVID were selected for generating a functional annotation chart using an unadjusted p-value threshold of 0.05.

References

1. Storey, J. D., and Tibshirani, R. (2003) *Methods Mol Biol* **224**, 149-157
2. Lin, R. C., Weeks, K. L., Gao, X. M., Williams, R. B., Bernardo, B. C., Kiriazis, H., Matthews, V. B., Woodcock, E. A., Bouwman, R. D., Mollica, J. P., Speirs, H. J., Dawes, I. W., Daly, R. J., Shioi, T., Izumo, S., Febbraio, M. A., Du, X. J., and McMullen, J. R. (2010) *Arterioscler Thromb Vasc Biol* **30**, 724-732
3. Waardenberg, A. J., Reverter, A., Wells, C. A., and Dalrymple, B. P. (2008) *BMC Syst Biol* **2**, 88
4. AC3D Manual. [http://www.ac3d.org/ac3d/download/ac3dman6b.pdf]
5. Ervasti, J. M. (2003) *J Biol Chem* **278**, 13591-13594
6. Bader, G. D., Donaldson, I., Wolting, C., Ouellette, B. F., Pawson, T., and Hogue, C. W. (2001) *Nucleic Acids Res* **29**, 242-245
7. Brancaccio, M., Guazzone, S., Menini, N., Sibona, E., Hirsch, E., De Andrea, M., Rocchi, M., Altruda, F., Tarone, G., and Silengo, L. (1999) *J Biol Chem* **274**, 29282-29288
8. Clark, K. A., McElhinny, A. S., Beckerle, M. C., and Gregorio, C. C. (2002) *Annu Rev Cell Dev Biol* **18**, 637-706
9. Davies, K. E., and Nowak, K. J. (2006) *Nat Rev Mol Cell Biol* **7**, 762-773
10. Li, J., Mayne, R., and Wu, C. (1999) *J Cell Biol* **147**, 1391-1398
11. Peri, S., Navarro, J. D., Amanchy, R., Kristiansen, T. Z., Jonnalagadda, C. K., Surendranath, V., Niranjan, V., Muthusamy, B., Gandhi, T. K., Gronborg, M., Ibarrola, N., Deshpande, N., Shanker, K., Shivashankar, H. N., Rashmi, B. P., Ramya, M. A., Zhao, Z., Chandrika, K. N., Padma, N., Harsha, H. C., Yatish, A. J., Kavitha, M. P., Menezes, M., Choudhury, D. R., Suresh, S., Ghosh, N., Saravana, R., Chandran, S., Krishna, S., Joy, M., Anand, S. K., Madavan, V., Joseph, A., Wong, G. W., Schiemann, W. P., Constantinescu, S. N., Huang, L., Khosravi-Far, R., Steen, H., Tewari, M., Ghaffari, S., Blobe, G. C., Dang, C. V., Garcia, J. G., Pevsner, J., Jensen, O. N., Roepstorff, P., Deshpande, K. S., Chinnaiyan, A. M., Hamosh, A., Chakravarti, A., and Pandey, A. (2003) *Genome Res* **13**, 2363-2371
12. Dennis, G., Jr., Sherman, B. T., Hosack, D. A., Yang, J., Gao, W., Lane, H. C., and Lempicki, R. A. (2003) *Genome Biol* **4**, P3

Supplementary Table I

Transcriptomics data of structural components highlighted from VMus3D analysis

Probeset ID	Gene Title	Gene Symbol	p-value (GenotypeX Treatment)	Mean(Ntg MI)	StdErr(Ntg MI)	Mean(Ntg Sham)	StdErr(Ntg Sham)
1426043_a_at	calpain 3	Capn3	4.28E-08	5.51415	0.0647418	5.5248	0.241134
1426778_at	dystroglycan 1	Dag1	0.000334167	10.8459	0.0621043	10.7952	0.0902402
1456131_x_at	dystroglycan 1	Dag1	0.00212354	9.07871	0.0982226	8.99774	0.081506
1426779_x_at	dystroglycan 1	Dag1	0.0027238	9.50981	0.0721527	9.39697	0.0672233
1447812_x_at	filamin C, gamma (actin binding protein 280)	Flnc	0.00566103	9.60395	0.130057	9.43989	0.104706
1449073_at	filamin C, gamma (actin binding protein 280)	Flnc	0.0123629	9.166	0.134049	8.8799	0.158383
1428183_at	ankyrin repeat domain 23	Ankrd23	7.70E-05	12.2842	0.114426	11.9257	0.274857
1434369_a_at	crystallin, alpha B	Cryab	9.39E-05	13.8655	0.0276797	13.868	0.0354249
1416455_a_at	crystallin, alpha B	Cryab	0.000212472	14.0607	0.0247307	13.9853	0.0796876
1423238_at	integrin beta 1 binding protein 2	Itgb1bp2	2.29E-06	11.2488	0.0801044	11.2098	0.0296426
1416752_at	LIM domain binding 3	Ldb3	0.000135416	12.1496	0.0530017	12.1842	0.0758853
1450828_at	synaptopodin 2	Synpo2	1.61E-06	8.3419	0.0680548	8.33541	0.180341
1452879_at	synaptopodin 2	Synpo2	1.85E-06	9.62731	0.0760364	9.48847	0.211305
1428295_at	synaptopodin 2-like	Synpo2l	2.56E-06	8.44492	0.158753	7.3885	0.190618
1447657_s_at	synaptopodin 2-like	Synpo2l	1.72E-05	11.8887	0.0817434	11.3438	0.236248
1447658_x_at	synaptopodin 2-like	Synpo2l	1.74E-05	11.6761	0.0813851	11.2043	0.150146
1451691_at	endothelin receptor type A	Ednra	2.63E-07	8.41884	0.0465864	8.31592	0.139176
1433525_at	endothelin receptor type A	Ednra	2.92E-07	8.53663	0.0250542	8.44326	0.130773
1460513_a_at	endothelin receptor type A	Ednra	0.000135476	7.15355	0.138155	7.24928	0.0903131
1440093_at	endothelin receptor type A	Ednra	0.00657795	5.48236	0.0833596	5.53833	0.104976
1452982_at	insulin-like growth factor I receptor	Igf1r	9.21E-09	8.00033	0.0855573	7.76825	0.0362324
1428967_at	insulin-like growth factor I receptor	Igf1r	0.000141843	5.58115	0.101729	5.44581	0.0507945
1426565_at	insulin-like growth factor I receptor	Igf1r	0.00134888	6.05605	0.0644206	6.05635	0.107263
1416657_at	thymoma viral proto-oncogene 1 /// similar to serine/threonine protein kinase	Akt1 /// LOC100047666	5.68E-08	8.41809	0.0374833	8.50504	0.0467761
1425711_a_at	thymoma viral proto-oncogene 1 /// similar to serine/threonine protein kinase	Akt1 /// LOC100047666	3.95E-05	8.24249	0.0457736	8.33733	0.0431031
1423104_at	insulin receptor substrate 1	Irs1	1.02E-09	10.2621	0.0781668	9.832	0.0836127
1448595_a_at	brain expressed gene 1	Bex1	6.81E-08	9.25782	0.142267	8.72464	0.710716
1460585_x_at	phosphatidylserine decarboxylase	Pisd	1.29E-07	9.54206	0.0288596	9.76653	0.0394972
1436944_x_at	RIKEN cDNA 4933439C20 gene /// phosphatidylserine decarboxylase pseudogene /// p	4933439C20Rik /// LOC236604 /// Pisd	0.0134103	8.50912	0.129309	8.34837	0.155516
1435425_at	RIKEN cDNA 4933439C20 gene /// phosphatidylserine decarboxylase	4933439C20Rik /// Pisd	0.0380703	6.15373	0.0224015	6.02385	0.0777252
1435426_s_at	RIKEN cDNA 4933439C20 gene /// phosphatidylserine decarboxylase	4933439C20Rik /// Pisd	0.64048	4.39328	0.116822	4.41508	0.173436
1456114_at	CDP-diacylglycerol synthase 1	Cds1	9.36E-06	5.75564	0.0619083	5.68678	0.0937261
1428680_at	CDP-diacylglycerol synthase 1	Cds1	0.000663067	5.30693	0.15611	5.10555	0.146384
1429862_at	phospholipase A2, group IVE	Pla2g4e	7.61E-06	5.82775	0.0458212	5.87353	0.0323166
1417814_at	phospholipase A2, group V	Pla2g5	1.65E-10	7.29717	0.044195	7.30125	0.0808955
1451041_at	Rho-associated coiled-coil containing protein kinase 2	Rock2	0.001769	9.1754	0.0771948	8.96659	0.120979
1423592_at	Rho-associated coiled-coil containing protein kinase 2	Rock2	0.0230171	8.84718	0.0581	8.54993	0.119985
1437670_x_at	CD151 antigen	Cd151	4.81E-05	11.3713	0.0337425	11.2194	0.106448
1456085_x_at	CD151 antigen	Cd151	8.36E-05	12.4217	0.0263093	12.2495	0.0897386
1424093_x_at	CD151 antigen	Cd151	0.000407447	10.6084	0.0188943	10.4973	0.106957
1451232_at	CD151 antigen	Cd151	0.00115452	10.5515	0.0258109	10.3678	0.138166

Gene Title	Mean(caPI3K MI)	StdErr(caPI3K MI)	Mean(caPI3K Sham)	StdErr(caPI3K Sham)	Mean(dnPI3K MI)	StdErr(dnPI3K MI)	Mean(dnPI3K Sham)	StdErr(dnPI3K Sham)
calpain 3	5.90039	0.154975	6.27228	0.156392	4.31838	0.0785752	4.38538	0.111122
dystroglycan 1	10.8636	0.0326845	11.0161	0.0244785	10.7537	0.0344861	10.5714	0.0260224
dystroglycan 1	9.08977	0.0457583	9.28701	0.0371078	8.86798	0.0758096	8.835	0.0488653
dystroglycan 1	9.49399	0.0342556	9.59743	0.0487006	9.32493	0.0592789	9.19277	0.0768127
filamin C, gamma (actin binding protein 280)	9.5739	0.0503767	9.73098	0.0638876	9.46736	0.122064	9.11437	0.0765404
filamin C, gamma (actin binding protein 280)	9.02814	0.0767191	9.21142	0.0556744	9.01783	0.101555	8.62634	0.0702658
ankyrin repeat domain 23	12.5057	0.0634164	12.5392	0.0619205	12.1349	0.130628	11.3132	0.0731619
crystallin, alpha B	14.016	0.0255856	14.0072	0.0202924	13.8547	0.0519824	13.7431	0.0228331
crystallin, alpha B	14.2079	0.0347028	14.2174	0.0234616	13.9739	0.0642016	13.808	0.0589953
integrin beta 1 binding protein 2	11.1671	0.0545525	11.3797	0.0256988	10.7693	0.0256103	11.0427	0.0596402
LIM domain binding 3	12.1535	0.0430578	12.3731	0.0449605	11.9322	0.0591673	11.9076	0.0535927
synaptopodin 2	8.54506	0.061612	8.85594	0.109851	7.86964	0.0344443	7.59211	0.118143
synaptopodin 2	9.73295	0.0594261	10.0289	0.0842387	9.08943	0.0652608	8.76629	0.0633889
synaptopodin 2-like	8.17318	0.147026	7.73945	0.146579	9.02553	0.221597	7.18905	0.106171
synaptopodin 2-like	11.8367	0.0544752	11.6068	0.0449332	12.0945	0.133528	10.8547	0.078513
synaptopodin 2-like	11.6195	0.0372828	11.4256	0.0564858	11.9868	0.137697	10.985	0.0745224
endothelin receptor type A	7.90806	0.0821815	8.01335	0.0611877	8.76515	0.141953	9.12006	0.0361452
endothelin receptor type A	8.0414	0.0597314	8.07011	0.0737053	8.85911	0.129568	9.17639	0.0861077
endothelin receptor type A	6.89479	0.0638794	7.0288	0.0645823	7.50467	0.183027	7.81065	0.0327946
endothelin receptor type A	5.42628	0.13	5.16744	0.100471	5.72153	0.165928	6.09618	0.231786
insulin-like growth factor I receptor	7.73208	0.0249535	7.55836	0.020818	8.55173	0.110356	8.39966	0.0655084
insulin-like growth factor I receptor	5.39923	0.0660306	5.13376	0.0574057	5.99898	0.171336	5.90485	0.13018
insulin-like growth factor I receptor	6.09811	0.0523289	5.91665	0.118937	6.60526	0.161164	6.52609	0.128079
thymoma viral proto-oncogene 1 /// similar to serine/threonine protein kinase	8.26244	0.0215843	8.19428	0.0447394	8.56832	0.011011	8.7142	0.0412696
thymoma viral proto-oncogene 1 /// similar to serine/threonine protein kinase	8.0403	0.106182	8.01213	0.0433489	8.30153	0.0401193	8.53888	0.0362117
insulin receptor substrate 1	9.69582	0.0756093	9.36007	0.0736976	10.8603	0.144029	10.8722	0.0718236
brain expressed gene 1	7.48161	0.132241	6.84461	0.376696	11.1785	0.370007	11.7645	0.0512192
phosphatidylserine decarboxylase	9.82328	0.0163945	9.89878	0.016656	9.34992	0.0470535	9.6082	0.0671671
RIKEN cDNA 4933439C20 gene /// phosphatidylserine decarboxylase pseudogene /// p	8.69649	0.0550043	8.43782	0.0644839	8.76807	0.0716533	8.23787	0.095918
RIKEN cDNA 4933439C20 gene /// phosphatidylserine decarboxylase	6.07043	0.0678648	6.27462	0.0300251	5.89214	0.126249	6.09039	0.0682769
RIKEN cDNA 4933439C20 gene /// phosphatidylserine decarboxylase	4.31641	0.0604491	4.16094	0.0568821	4.34412	0.119071	4.28823	0.086738
CDP-diacylglycerol synthase 1	5.89724	0.0842263	6.20452	0.114794	5.54305	0.0513161	5.21855	0.101993
CDP-diacylglycerol synthase 1	5.28577	0.159275	5.64221	0.147127	4.62976	0.2426	4.50397	0.0547029
phospholipase A2, group IVE	5.88706	0.0323284	6.10066	0.0360656	5.50309	0.0844635	5.50406	0.0993139
phospholipase A2, group V	7.69497	0.0799816	8.09725	0.068896	5.15422	0.24367	5.69737	0.248268
Rho-associated coiled-coil containing protein kinase 2	9.10078	0.0583812	9.22938	0.0386874	9.04613	0.0300576	8.71661	0.0808753
Rho-associated coiled-coil containing protein kinase 2	8.71848	0.0649425	8.70939	0.066943	8.66298	0.0557699	8.45294	0.0606851
CD151 antigen	11.4739	0.0237709	11.4234	0.0282717	11.2239	0.0518427	10.9719	0.036779
CD151 antigen	12.4637	0.0421009	12.4753	0.0232763	12.3007	0.0584263	12.0646	0.00463218
CD151 antigen	10.6014	0.0355254	10.6827	0.0337135	10.4056	0.0580436	10.2609	0.0248515
CD151 antigen	10.5315	0.034843	10.6185	0.0470119	10.3433	0.0461168	10.1673	0.0144076

Gene Title	p-value(Ntg MI vs. Ntg Sham)	Ratio(Ntg MI vs. Ntg Sham)	Fold-Change(Ntg MI vs. Ntg Sham)	Fold-Change(Ntg MI vs. Ntg Sham) (Description)	p-value(caPI3K MI vs. Ntg Sham)	Ratio(caPI3K MI vs. Ntg Sham)
calpain 3	0.959677	0.992649	-1.00741	Ntg MI down vs Ntg Sham	0.087194	1.29738
dystroglycan 1	0.490306	1.03575	1.03575	Ntg MI up vs Ntg Sham	0.354942	1.0485
dystroglycan 1	0.412107	1.05773	1.05773	Ntg MI up vs Ntg Sham	0.352568	1.06587
dystroglycan 1	0.210798	1.08135	1.08135	Ntg MI up vs Ntg Sham	0.279246	1.06956
filamin C, gamma (actin binding protein 280)	0.242365	1.12043	1.12043	Ntg MI up vs Ntg Sham	0.336517	1.09734
filamin C, gamma (actin binding protein 280)	0.0721608	1.21934	1.21934	Ntg MI up vs Ntg Sham	0.335405	1.10821
ankyrin repeat domain 23	0.0885124	1.28211	1.28211	Ntg MI up vs Ntg Sham	0.00927118	1.4949
crystallin, alpha B	0.957131	0.998269	-1.00173	Ntg MI down vs Ntg Sham	0.00467274	1.10805
crystallin, alpha B	0.320327	1.05363	1.05363	Ntg MI up vs Ntg Sham	0.00739846	1.16679
integrin beta 1 binding protein 2	0.589347	1.02744	1.02744	Ntg MI up vs Ntg Sham	0.555802	0.97087
LIM domain binding 3	0.667835	0.976336	-1.02424	Ntg MI down vs Ntg Sham	0.702823	0.978945
synaptopodin 2	0.966171	1.0045	1.0045	Ntg MI up vs Ntg Sham	0.181228	1.15641
synaptopodin 2	0.373208	1.10101	1.10101	Ntg MI up vs Ntg Sham	0.125202	1.18467
synaptopodin 2-like	0.000274371	2.07975	2.07975	Ntg MI up vs Ntg Sham	0.00359905	1.7227
synaptopodin 2-like	0.00590818	1.45892	1.45892	Ntg MI up vs Ntg Sham	0.011274	1.40727
synaptopodin 2-like	0.00329024	1.38693	1.38693	Ntg MI up vs Ntg Sham	0.00802831	1.33355
endothelin receptor type A	0.450897	1.07394	1.07394	Ntg MI up vs Ntg Sham	0.0068272	0.753738
endothelin receptor type A	0.482843	1.06686	1.06686	Ntg MI up vs Ntg Sham	0.00639592	0.756878
endothelin receptor type A	0.538932	0.9358	-1.0686	Ntg MI down vs Ntg Sham	0.0323256	0.78215
endothelin receptor type A	0.788097	0.961954	-1.03955	Ntg MI down vs Ntg Sham	0.591619	0.925279
insulin-like growth factor I receptor	0.0230004	1.17452	1.17452	Ntg MI up vs Ntg Sham	0.70306	0.975242
insulin-like growth factor I receptor	0.376695	1.09835	1.09835	Ntg MI up vs Ntg Sham	0.758686	0.968232
insulin-like growth factor I receptor	0.99848	0.999788	-1.00021	Ntg MI down vs Ntg Sham	0.794571	1.02937
thymoma viral proto-oncogene 1 /// similar to serine/threonine protein kinase	0.107108	0.941511	-1.06212	Ntg MI down vs Ntg Sham	0.000166308	0.845218
thymoma viral proto-oncogene 1 /// similar to serine/threonine protein kinase	0.260921	0.936378	-1.06795	Ntg MI down vs Ntg Sham	0.00189212	0.813923
insulin receptor substrate 1	0.00375532	1.34732	1.34732	Ntg MI up vs Ntg Sham	0.306146	0.909922
brain expressed gene 1	0.322551	1.44711	1.44711	Ntg MI up vs Ntg Sham	0.029081	0.422484
phosphatidylserine decarboxylase	0.000928897	0.855912	-1.16834	Ntg MI down vs Ntg Sham	0.330658	1.04012
RIKEN cDNA 4933439C20 gene /// phosphatidylserine decarboxylase pseudogene /// p	0.279759	1.11787	1.11787	Ntg MI up vs Ntg Sham	0.0266871	1.2729
RIKEN cDNA 4933439C20 gene /// phosphatidylserine decarboxylase	0.229136	1.0942	1.0942	Ntg MI up vs Ntg Sham	0.6606	1.03281
RIKEN cDNA 4933439C20 gene /// phosphatidylserine decarboxylase	0.889909	0.985005	-1.01522	Ntg MI down vs Ntg Sham	0.533104	0.933895
CDP-diacylglycerol synthase 1	0.584702	1.04889	1.04889	Ntg MI up vs Ntg Sham	0.106153	1.15706
CDP-diacylglycerol synthase 1	0.386822	1.1498	1.1498	Ntg MI up vs Ntg Sham	0.437703	1.13305
phospholipase A2, group IVE	0.603403	0.968764	-1.03224	Ntg MI down vs Ntg Sham	0.877578	1.00942
phospholipase A2, group V	0.985184	0.997178	-1.00283	Ntg MI down vs Ntg Sham	0.0856921	1.31378
Rho-associated coiled-coil containing protein kinase 2	0.0616913	1.15573	1.15573	Ntg MI up vs Ntg Sham	0.216605	1.09748
Rho-associated coiled-coil containing protein kinase 2	0.0112703	1.2288	1.2288	Ntg MI up vs Ntg Sham	0.126863	1.12392
CD151 antigen	0.0647216	1.11101	1.11101	Ntg MI up vs Ntg Sham	0.00400402	1.19294
CD151 antigen	0.0234334	1.12672	1.12672	Ntg MI up vs Ntg Sham	0.00644296	1.16002
CD151 antigen	0.170669	1.08005	1.08005	Ntg MI up vs Ntg Sham	0.197818	1.07482
CD151 antigen	0.0617712	1.13579	1.13579	Ntg MI up vs Ntg Sham	0.0929831	1.12008

Fold-Change(caPI3K MI vs. Ntg Sham)	Fold-Change(caPI3K MI vs. Ntg Sham) (Description)	p-value(caPI3K Shar	Ratio(caPI3K Sham vs. Ntg Sham)	Fold-Change(caPI3K Sham vs. Ntg Sham)	Fold-Change(caPI3K Sham vs. Ntg Sham) (Description)	p-value(dnPI3K MI vs. Ntg Sham)	Ratio(dnPI3K MI vs. Ntg Sham)
1.29738	caPI3K MI up vs Ntg Sham	0.0020471	1.67886	1.67886	caPI3K Sham up vs Ntg Sham	1.67E-05	0.433343
1.0485	caPI3K MI up vs Ntg Sham	0.00660576	1.16544	1.16544	caPI3K Sham up vs Ntg Sham	0.570581	0.971594
1.06587	caPI3K MI up vs Ntg Sham	0.00769053	1.22202	1.22202	caPI3K Sham up vs Ntg Sham	0.195128	0.913983
1.06956	caPI3K MI up vs Ntg Sham	0.0332756	1.14906	1.14906	caPI3K Sham up vs Ntg Sham	0.418278	0.951294
1.09734	caPI3K MI up vs Ntg Sham	0.0458601	1.22356	1.22356	caPI3K Sham up vs Ntg Sham	0.841853	1.01923
1.10821	caPI3K MI up vs Ntg Sham	0.0400155	1.25833	1.25833	caPI3K Sham up vs Ntg Sham	0.369281	1.10032
1.4949	caPI3K MI up vs Ntg Sham	0.00643256	1.52999	1.52999	caPI3K Sham up vs Ntg Sham	0.307209	1.15607
1.10805	caPI3K MI up vs Ntg Sham	0.00710559	1.10133	1.10133	caPI3K Sham up vs Ntg Sham	0.774734	0.990806
1.16679	caPI3K MI up vs Ntg Sham	0.00559181	1.17446	1.17446	caPI3K Sham up vs Ntg Sham	0.878618	0.992112
-1.03	caPI3K MI down vs Ntg Sham	0.0279645	1.12494	1.12494	caPI3K Sham up vs Ntg Sham	7.50E-06	0.736866
-1.02151	caPI3K MI down vs Ntg Sham	0.0282896	1.13987	1.13987	caPI3K Sham up vs Ntg Sham	0.00516662	0.839746
1.15641	caPI3K MI up vs Ntg Sham	0.00283603	1.43448	1.43448	caPI3K Sham up vs Ntg Sham	0.0063156	0.724084
1.18467	caPI3K MI up vs Ntg Sham	0.00226408	1.45439	1.45439	caPI3K Sham up vs Ntg Sham	0.0171772	0.75836
1.7227	caPI3K MI up vs Ntg Sham	0.151895	1.27539	1.27539	caPI3K Sham up vs Ntg Sham	1.61E-06	3.11024
1.40727	caPI3K MI up vs Ntg Sham	0.149345	1.19999	1.19999	caPI3K Sham up vs Ntg Sham	0.000431716	1.68267
1.33355	caPI3K MI up vs Ntg Sham	0.129576	1.16584	1.16584	caPI3K Sham up vs Ntg Sham	2.50E-05	1.72023
-1.32672	caPI3K MI down vs Ntg Sham	0.0360276	0.810805	-1.23334	caPI3K Sham down vs Ntg Sham	0.00345525	1.36531
-1.32122	caPI3K MI down vs Ntg Sham	0.0103192	0.772093	-1.29518	caPI3K Sham down vs Ntg Sham	0.00505566	1.33408
-1.27853	caPI3K MI down vs Ntg Sham	0.166294	0.858281	-1.16512	caPI3K Sham down vs Ntg Sham	0.111991	1.19366
-1.08076	caPI3K MI down vs Ntg Sham	0.0873173	0.773305	-1.29315	caPI3K Sham down vs Ntg Sham	0.383553	1.1354
-1.02539	caPI3K MI down vs Ntg Sham	0.0373653	0.864603	-1.1566	caPI3K Sham down vs Ntg Sham	1.24E-07	1.72128
-1.03281	caPI3K MI down vs Ntg Sham	0.0510981	0.805498	-1.24147	caPI3K Sham down vs Ntg Sham	0.00162164	1.46731
1.02937	caPI3K MI up vs Ntg Sham	0.388321	0.907705	-1.10168	caPI3K Sham down vs Ntg Sham	0.00271171	1.46297
-1.18313	caPI3K MI down vs Ntg Sham	9.94E-06	0.806218	-1.24036	caPI3K Sham down vs Ntg Sham	0.233007	1.04483
-1.22862	caPI3K MI down vs Ntg Sham	0.000877869	0.798188	-1.25284	caPI3K Sham down vs Ntg Sham	0.666508	0.975492
-1.099	caPI3K MI down vs Ntg Sham	0.00183141	0.720996	-1.38697	caPI3K Sham down vs Ntg Sham	2.66E-07	2.03969
-2.36696	caPI3K MI down vs Ntg Sham	0.00210888	0.271678	-3.68083	caPI3K Sham down vs Ntg Sham	0.000185885	5.47878
1.04012	caPI3K MI up vs Ntg Sham	0.0316342	1.09601	1.09601	caPI3K Sham up vs Ntg Sham	8.17E-07	0.749183
1.2729	caPI3K MI up vs Ntg Sham	0.54296	1.06396	1.06396	caPI3K Sham up vs Ntg Sham	0.0093501	1.33765
1.03281	caPI3K MI up vs Ntg Sham	0.027219	1.18984	1.18984	caPI3K Sham up vs Ntg Sham	0.222879	0.912749
-1.07078	caPI3K MI down vs Ntg Sham	0.119025	0.838487	-1.19262	caPI3K Sham down vs Ntg Sham	0.653136	0.952008
1.15706	caPI3K MI up vs Ntg Sham	0.000557073	1.43171	1.43171	caPI3K Sham up vs Ntg Sham	0.260518	0.905171
1.13305	caPI3K MI up vs Ntg Sham	0.0295517	1.45061	1.45061	caPI3K Sham up vs Ntg Sham	0.0505336	0.719072
1.00942	caPI3K MI up vs Ntg Sham	0.0172297	1.1705	1.1705	caPI3K Sham up vs Ntg Sham	0.000451922	0.773545
1.31378	caPI3K MI up vs Ntg Sham	0.00172781	1.73628	1.73628	caPI3K Sham up vs Ntg Sham	1.02E-08	0.225778
1.09748	caPI3K MI up vs Ntg Sham	0.0219503	1.1998	1.1998	caPI3K Sham up vs Ntg Sham	0.457635	1.05668
1.12392	caPI3K MI up vs Ntg Sham	0.147305	1.11687	1.11687	caPI3K Sham up vs Ntg Sham	0.297191	1.08151
1.19294	caPI3K MI up vs Ntg Sham	0.0165252	1.15191	1.15191	caPI3K Sham up vs Ntg Sham	0.954406	1.00311
1.16002	caPI3K MI up vs Ntg Sham	0.00446375	1.16941	1.16941	caPI3K Sham up vs Ntg Sham	0.47129	1.03609
1.07482	caPI3K MI up vs Ntg Sham	0.0284879	1.13713	1.13713	caPI3K Sham up vs Ntg Sham	0.253802	0.938368
1.12008	caPI3K MI up vs Ntg Sham	0.0141209	1.1897	1.1897	caPI3K Sham up vs Ntg Sham	0.793106	0.983127

Fold-Change(dnPI3K MI vs. Ntg Sham)	Fold-Change(dnPI3K MI vs. Ntg Sham) (Description)	p-value(dnPI3K Sham vs. Ntg Sham)	Ratio(dnPI3K Sham vs. Ntg Sham)	Fold-Change (dnPI3K Sham vs. Ntg Sham)	Fold-Change(dnPI3K Sham vs. Ntg Sham) (Description)	F(GenotypeX Treatment)	F(Error)	Entrez Gene
-2.30764	dnPI3K MI down vs Ntg Sham	3.27E-05	0.453944	-2.20291	dnPI3K Sham down vs Ntg Sham	29.6911	1	12335
-1.02924	dnPI3K MI down vs Ntg Sham	0.00603025	0.856262	-1.16787	dnPI3K Sham down vs Ntg Sham	8.26158	1	13138
-1.09411	dnPI3K MI down vs Ntg Sham	0.108717	0.893322	-1.11942	dnPI3K Sham down vs Ntg Sham	5.90263	1	13138
-1.0512	dnPI3K MI down vs Ntg Sham	0.0304881	0.868022	-1.15205	dnPI3K Sham down vs Ntg Sham	5.61878	1	13138
1.01923	dnPI3K MI up vs Ntg Sham	0.0275093	0.798012	-1.25311	dnPI3K Sham down vs Ntg Sham	4.82554	1	68794
1.10032	dnPI3K MI up vs Ntg Sham	0.107678	0.838821	-1.19215	dnPI3K Sham down vs Ntg Sham	4.04068	1	68794
1.15607	dnPI3K MI up vs Ntg Sham	0.00650534	0.654062	-1.52891	dnPI3K Sham down vs Ntg Sham	10.499	1	78321
-1.00928	dnPI3K MI down vs Ntg Sham	0.0139476	0.917068	-1.09043	dnPI3K Sham down vs Ntg Sham	10.1739	1	12955
-1.00795	dnPI3K MI down vs Ntg Sham	0.0271673	0.884326	-1.1308	dnPI3K Sham down vs Ntg Sham	8.91396	1	12955
-1.3571	dnPI3K MI down vs Ntg Sham	0.0302669	0.890631	-1.1228	dnPI3K Sham down vs Ntg Sham	17.5673	1	26549
-1.19084	dnPI3K MI down vs Ntg Sham	0.00260277	0.825563	-1.21129	dnPI3K Sham down vs Ntg Sham	9.59542	1	24131
-1.38105	dnPI3K MI down vs Ntg Sham	0.000107764	0.59737	-1.674	dnPI3K Sham down vs Ntg Sham	18.4359	1	118449
-1.31863	dnPI3K MI down vs Ntg Sham	0.000159806	0.606178	-1.64968	dnPI3K Sham down vs Ntg Sham	18.0924	1	118449
3.11024	dnPI3K MI up vs Ntg Sham	0.40626	0.870881	-1.14826	dnPI3K Sham down vs Ntg Sham	17.2989	1	68760
1.68267	dnPI3K MI up vs Ntg Sham	0.0118235	0.712506	-1.4035	dnPI3K Sham down vs Ntg Sham	13.1824	1	68760
1.72023	dnPI3K MI up vs Ntg Sham	0.133106	0.859027	-1.16411	dnPI3K Sham down vs Ntg Sham	13.1568	1	68760
1.36531	dnPI3K MI up vs Ntg Sham	1.08E-05	1.7461	1.7461	dnPI3K Sham up vs Ntg Sham	23.4956	1	13617
1.33408	dnPI3K MI up vs Ntg Sham	2.44E-05	1.66224	1.66224	dnPI3K Sham up vs Ntg Sham	23.1712	1	13617
1.19366	dnPI3K MI up vs Ntg Sham	0.00173923	1.47567	1.47567	dnPI3K Sham up vs Ntg Sham	9.59472	1	13617
1.1354	dnPI3K MI up vs Ntg Sham	0.0140511	1.47208	1.47208	dnPI3K Sham up vs Ntg Sham	4.66994	1	13617
1.72128	dnPI3K MI up vs Ntg Sham	2.46E-06	1.54908	1.54908	dnPI3K Sham up vs Ntg Sham	35.9949	1	16001
1.46731	dnPI3K MI up vs Ntg Sham	0.00653683	1.37463	1.37463	dnPI3K Sham up vs Ntg Sham	9.52372	1	16001
1.46297	dnPI3K MI up vs Ntg Sham	0.00815837	1.38486	1.38486	dnPI3K Sham up vs Ntg Sham	6.43945	1	16001
1.04483	dnPI3K MI up vs Ntg Sham	0.000703179	1.15601	1.15601	dnPI3K Sham up vs Ntg Sham	28.6392	1	100047666 /// 11651
-1.02512	dnPI3K MI down vs Ntg Sham	0.0239006	1.14993	1.14993	dnPI3K Sham up vs Ntg Sham	11.6373	1	100047666 /// 11651
2.03969	dnPI3K MI up vs Ntg Sham	2.26E-07	2.05658	2.05658	dnPI3K Sham up vs Ntg Sham	47.1402	1	16367
5.47878	dnPI3K MI up vs Ntg Sham	1.70E-05	8.22394	8.22394	dnPI3K Sham up vs Ntg Sham	27.9818	1	19716
-1.33479	dnPI3K MI down vs Ntg Sham	0.0121048	0.896062	-1.11599	dnPI3K Sham down vs Ntg Sham	25.7804	1	320951
1.33765	dnPI3K MI up vs Ntg Sham	0.453607	0.92627	-1.0796	dnPI3K Sham down vs Ntg Sham	3.96236	1	236604 /// 320951 ///
-1.09559	dnPI3K MI down vs Ntg Sham	0.531622	1.0472	1.0472	dnPI3K Sham up vs Ntg Sham	3.00815	1	320951 /// 66776
-1.05041	dnPI3K MI down vs Ntg Sham	0.424605	0.915829	-1.09191	dnPI3K Sham down vs Ntg Sham	0.685539	1	320951 /// 66776
-1.10476	dnPI3K MI down vs Ntg Sham	0.00135782	0.722851	-1.38341	dnPI3K Sham down vs Ntg Sham	14.4046	1	74596
-1.39068	dnPI3K MI down vs Ntg Sham	0.0163054	0.65903	-1.51738	dnPI3K Sham down vs Ntg Sham	7.33288	1	74596
-1.29275	dnPI3K MI down vs Ntg Sham	0.000463295	0.774065	-1.29188	dnPI3K Sham down vs Ntg Sham	14.84	1	329502
-4.42913	dnPI3K MI down vs Ntg Sham	7.21E-07	0.328992	-3.03959	dnPI3K Sham down vs Ntg Sham	58.6466	1	18784
1.05668	dnPI3K MI up vs Ntg Sham	0.0282571	0.84091	-1.18919	dnPI3K Sham down vs Ntg Sham	6.11565	1	19878
1.08151	dnPI3K MI up vs Ntg Sham	0.369197	0.934983	-1.06954	dnPI3K Sham down vs Ntg Sham	3.45707	1	19878
1.00311	dnPI3K MI up vs Ntg Sham	0.00489994	0.842384	-1.18711	dnPI3K Sham down vs Ntg Sham	11.2937	1	12476
1.03609	dnPI3K MI up vs Ntg Sham	0.0159089	0.879664	-1.1368	dnPI3K Sham down vs Ntg Sham	10.3634	1	12476
-1.06568	dnPI3K MI down vs Ntg Sham	0.00709198	0.848846	-1.17807	dnPI3K Sham down vs Ntg Sham	7.98581	1	12476
-1.01716	dnPI3K MI down vs Ntg Sham	0.0432581	0.870234	-1.14912	dnPI3K Sham down vs Ntg Sham	6.62948	1	12476

Gene Ontology Biological Process	Gene Ontology Cellular Component	Gene Ontology Molecular Function	MGI Name	
0006006 // glucose metabolic process // infer	0005622 // intracellular // inferred from elec	0004197 // cysteine-type endopeptidase a	107437	
0002011 // morphogenesis of an epithelial she	0005576 // extracellular region // inferred fr	0005509 // calcium ion binding // inferred	101864	
0002011 // morphogenesis of an epithelial she	0005576 // extracellular region // inferred fr	0005509 // calcium ion binding // inferred	101864	
0002011 // morphogenesis of an epithelial she	0005576 // extracellular region // inferred fr	0005509 // calcium ion binding // inferred	101864	
0030029 // actin filament-based process // tra	0005737 // cytoplasm // inferred from electr	0003779 // actin binding // traceable auth	95557	
0030029 // actin filament-based process // tra	0005737 // cytoplasm // inferred from electr	0003779 // actin binding // traceable auth	95557	
0006631 // fatty acid metabolic process // inf	0005634 // nucleus // inferred from direct a	---	1925571	
0007169 // transmembrane receptor protein t	0005625 // soluble fraction // inferred from	0005212 // structural constituent of eye le	88516	
0007169 // transmembrane receptor protein t	0005625 // soluble fraction // inferred from	0005212 // structural constituent of eye le	88516	
0007229 // integrin-mediated signaling pathw	0030018 // Z disc // inferred from direct ass	0005509 // calcium ion binding // inferred	1353420	
---	0005737 // cytoplasm // inferred from electr	0005080 // protein kinase C binding // inf	1344412	
---	0005634 // nucleus // inferred from electron	0003779 // actin binding // not recorded /	2153070	
---	0005634 // nucleus // inferred from electron	0003779 // actin binding // not recorded /	2153070	
---	0005737 // cytoplasm // inferred from electr	0003779 // actin binding // inferred from	1916010	
---	0005737 // cytoplasm // inferred from electr	0003779 // actin binding // inferred from	1916010	
---	0005737 // cytoplasm // inferred from electr	0003779 // actin binding // inferred from	1916010	
0001569 // patterning of blood vessels // infe	0005886 // plasma membrane // inferred fro	0001584 // rhodopsin-like receptor activit	105923	
0001569 // patterning of blood vessels // infe	0005886 // plasma membrane // inferred fro	0001584 // rhodopsin-like receptor activit	---	
0001569 // patterning of blood vessels // infe	0005886 // plasma membrane // inferred fro	0001584 // rhodopsin-like receptor activit	105923	
0001569 // patterning of blood vessels // infe	0005886 // plasma membrane // inferred fro	0001584 // rhodopsin-like receptor activit	105923	
0006468 // protein amino acid phosphorylatio	0016020 // membrane // inferred from elect	0000166 // nucleotide binding // inferred	---	
0006468 // protein amino acid phosphorylatio	0016020 // membrane // inferred from elect	0000166 // nucleotide binding // inferred	96433	
0006468 // protein amino acid phosphorylatio	0016020 // membrane // inferred from elect	0000166 // nucleotide binding // inferred	96433	
0000060 // protein import into nucleus, transl	0005634 // nucleus // inferred from electron	0000166 // nucleotide binding // inferred	87986 /// 87986	
0000060 // protein import into nucleus, transl	0005634 // nucleus // inferred from electron	0000166 // nucleotide binding // inferred	87986 /// 87986	
0002053 // positive regulation of mesenchym	0005634 // nucleus // inferred from direct a	0004871 // signal transducer activity // in	---	
0002052 // positive regulation of neuroblast p	0005634 // nucleus // inferred from direct a	0005515 // protein binding // inferred fro	1328321	
0008654 // phospholipid biosynthetic process	0005739 // mitochondrion // inferred from e	0004609 // phosphatidylserine decarboxyl	2445114	
0008654 // phospholipid biosynthetic process	0005739 // mitochondrion // inferred from e	0004609 // phosphatidylserine decarboxyl	1914026 /// 1914026 /// 1914026	
0008654 // phospholipid biosynthetic process	0005739 // mitochondrion // inferred from e	0004609 // phosphatidylserine decarboxyl	1914026 /// 1914026	
0008654 // phospholipid biosynthetic process	0005739 // mitochondrion // inferred from e	0004609 // phosphatidylserine decarboxyl	1914026 /// 1914026	
0008654 // phospholipid biosynthetic process	0005783 // endoplasmic reticulum // inferre	0000287 // magnesium ion binding // infe	1921846	
0008654 // phospholipid biosynthetic process	0005783 // endoplasmic reticulum // inferre	0000287 // magnesium ion binding // infe	1921846	
0008152 // metabolic process // inferred from	0005737 // cytoplasm // inferred from direc	0004620 // phospholipase activity // infer	1919144	
0006644 // phospholipid metabolic process //	0005576 // extracellular region // inferred fr	0004623 // phospholipase A2 activity // in	101899	
0000910 // cytokinesis // inferred from electr	0005622 // intracellular // inferred from elec	0000166 // nucleotide binding // inferred	---	
0000910 // cytokinesis // inferred from electr	0005622 // intracellular // inferred from elec	0000166 // nucleotide binding // inferred	107926	
0001701 // in utero embryonic development /	0005634 // nucleus // inferred from direct a	0003676 // nucleic acid binding // inferred	1096360	
0001701 // in utero embryonic development /	0005634 // nucleus // inferred from direct a	0003676 // nucleic acid binding // inferred	1096360	
0007601 // visual perception // inferred from	0016020 // membrane // inferred from elect	---	1096360	
0007601 // visual perception // inferred from	0016020 // membrane // inferred from elect	---	1096360	

Supplementary Table II												
Category	Term	Count	%	PValue	Genes	List Total	Pop Hits	Pop Total	Fold Enrichment	Bonferroni	Benjamini	FDR
KEGG_PATHWAY	mmu03010:Ribosome	18	2.17918	3.85E-08	RPL18,RPS9,RPS4X,RPS5,RPS7,RPS3,RPS25,RPS27,RPL7,RPL23,RPL18A,RPS17,RPLP0,RPLP1,RPS15,RPL11,RPL12,RPS21	225	89	5738	5.157752809	5.82E-06	5.82E-06	4.61E-05
BIOCARTA	m_igf1rPathway:Multiple antiapoptotic pathways from IGF-1R signaling lead to BAD phosphorylation	5	0.60533	0.004093	IGF1R,GRB2,RAF1,BAD,IRS1	44	19	1171	7.003588517	0.36308614	0.3630861	4.527815
KEGG_PATHWAY	mmu04510:Focal adhesion	16	1.93705	0.010107	MYL7,ROCK2,GRB2,MYLK3,RAF1,BAD,MAPK10,FLNC,IGF1R,PPP1CA,LAMB3,CCND2,ITGB6,LAMB1-1,EGF,COL11A1	225	198	5738	2.060785634	0.78430494	0.5355702	11.43605
KEGG_PATHWAY	mmu04910:Insulin signaling pathway	12	1.45278	0.018519	PPP1R3D,PPP1CA,EIF4EBP1,PHKB,PYGL,GRB2,PRKAG1,FASN,RAF1,MAPK10,BAD,IRS1	225	138	5738	2.217584541	0.94054618	0.6097048	20.02652
BIOCARTA	m_igf1Pathway:IGF-1 Signaling Pathway	4	0.48426	0.038674	IGF1R,GRB2,RAF1,IRS1	44	21	1171	5.069264069	0.98694498	0.8857414	35.9574
BIOCARTA	m_il2rbPathway:IL-2 Receptor Beta Chain in T cell Activation	5	0.60533	0.039473	GRB2,RAF1,JAK1,BAD,IRS1	44	36	1171	3.696338384	0.98808577	0.7716039	36.55606
KEGG_PATHWAY	mmu00564:Glycerophospholipid metabolism	7	0.84746	0.045646	DGKZ,PCYT1A,PISD,CDS1,CHPT1,PLA2G4E,PLA2G5	225	67	5738	2.664411277	0.99913676	0.8285912	42.79696

Supplementary Table III: Boolean descriptive index

Descriptive logic (1-2-3-4-5)

- this describes the comparisons performed and number (1-5) indicates each comparison

o 1 = capi3k/dnpi3k Sham vs. Ntg Sham
o 2 = capi3k/dnpi3k MI vs. Ntg MI
o 3 = Sham only (i.e. significant only in sham)
o 4 = MI only (i.e. significant only in MI)
o 5 = Sham and MI (significant in both)

1 = Boolean descriptor for presence (being significant and present) of pattern of interest and A, B, C, D = pattern where necessary. (0 = absence of pattern/significance).

- A = up-down (reciprocal)
- B = down-up (reciprocal)
- C = up-up (uni-directional)
- D = down-down (uni-directional)

IDENTIFIER	Descriptive_logic(1-2-3-4-5)
0610009B22Rik	'01A000'
0610009L18Rik	'01A000'
Asb5	'01A000'
Bphl	'01A000'
Cacybp	'01A000'
Chpt1	'01A000'
Dhx32	'01A000'
Gm410	'01A000'
Hspe1	'01A000'
LOC100044161 /// Sema3a	'01A000'
Lyrm5	'01A000'
Ormdl1	'01A000'
Amn1	'01A001A'
Cops7b	'01A001A'
Skp1a	'01A001A'
1700025G04Rik /// LOC545371	'01B000'
Ahnak	'01B000'
B4galt6 /// LOC675709	'01B000'
Ccnd2	'01B000'
Etv5	'01B000'
Fgl2	'01B000'
Gnptab	'01B000'
Hn1	'01B000'
Ik	'01B000'
LOC100046056 /// Pbxip1	'01B000'
Ndrg4	'01B000'
Tac1	'01B000'
Tmbim1	'01B000'
Upp1	'01B000'

Gcnt2	'01B001B'
Myo1c	'01B001B'
Nrd1	'01B001B'
Rab17	'01B001B'
Rusc2	'01B001B'
Spats1	'01B001B'
4921527H02Rik	'01C000'
4930534B04Rik	'01C000'
Aen	'01C000'
Ard1a	'01C000'
Atp5o /// LOC100047429	'01C000'
Bbox1	'01C000'
Ckap2l	'01C000'
Cmtm8	'01C000'
Cnot2	'01C000'
Dynlrb1	'01C000'
Gstm5	'01C000'
L2hgdh	'01C000'
LOC100047123	'01C000'
LOC100049077	'01C000'
Mapbpip	'01C000'
Mipol1	'01C000'
Mrpl35	'01C000'
Mrpl48	'01C000'
Myl7	'01C000'
Naif1	'01C000'
Prkag1	'01C000'
Prps1	'01C000'
Ptgfr	'01C000'
Sec14l4	'01C000'
Sfxn4	'01C000'
Sln	'01C000'
Sync	'01C000'
Tmem205	'01C000'
Ubxn6	'01C000'
Utp20	'01C000'
Zfp454	'01C000'
0610010D20Rik	'01C001C'
0610011L14Rik	'01C001C'
1190005F20Rik	'01C001C'
1700040L02Rik	'01C001C'
2010001A14Rik	'01C001C'
2010005J08Rik	'01C001C'
2810016G10Rik	'01C001C'
4921504P05Rik	'01C001C'
4921517D16Rik	'01C001C'
4921525O09Rik	'01C001C'
4933416E03Rik	'01C001C'
5930434B04Rik /// LOC100047034	'01C001C'
6030422H21Rik	'01C001C'

6030460B20Rik	'01C001C'
9130221J17Rik	'01C001C'
Abcf2	'01C001C'
Abcf3	'01C001C'
Acot6	'01C001C'
Adrbk1	'01C001C'
Apip /// LOC100044135	'01C001C'
Atp5c1	'01C001C'
Atp5g1 /// ENSMUSG00000058357	'01C001C'
Aven	'01C001C'
Bat2	'01C001C'
BC024814	'01C001C'
Bzw2	'01C001C'
C78444	'01C001C'
C85492	'01C001C'
Caskin1	'01C001C'
Ccdc64b	'01C001C'
Ccdc97	'01C001C'
Cdc37l1	'01C001C'
Cisd3	'01C001C'
Cmtm2b	'01C001C'
Col11a1	'01C001C'
Coq6	'01C001C'
Cox10	'01C001C'
Cyp2d34	'01C001C'
Dennd4c	'01C001C'
Dgat1	'01C001C'
Dgcr6	'01C001C'
Eef2k	'01C001C'
Efr3a	'01C001C'
EG624219	'01C001C'
Eif2b4	'01C001C'
Eif3m	'01C001C'
ENSMUSG00000074243 /// Josd1	'01C001C'
Epha4	'01C001C'
Exosc7	'01C001C'
F13b	'01C001C'
Fam174b	'01C001C'
Fn3k	'01C001C'
Ftsj1 /// LOC100044636	'01C001C'
Fxn	'01C001C'
Gspt2	'01C001C'
H2-Ke2	'01C001C'
Hmox2	'01C001C'
Hmx3	'01C001C'
Hoxd13	'01C001C'
Kcnj1	'01C001C'
Kcnk3	'01C001C'
Khdrbs3	'01C001C'
Krtap13-1	'01C001C'

Lce1b	'01C001C'
LOC100045988	'01C001C'
LOC100048812 /// Spag7	'01C001C'
LOC629952 /// OTTMUSG00000002349 /// Ppih	'01C001C'
Lrpprc	'01C001C'
Mc2r	'01C001C'
Mecr	'01C001C'
Mrpl11	'01C001C'
Mrpl54	'01C001C'
Mrrf	'01C001C'
Msh6	'01C001C'
Mybphl	'01C001C'
Myg1	'01C001C'
Ndufa11	'01C001C'
Ndufa12	'01C001C'
Ndufa13	'01C001C'
Ndufs6	'01C001C'
Ndufs7	'01C001C'
Nqo2	'01C001C'
Nudt14	'01C001C'
Pctp	'01C001C'
Pcyt1a	'01C001C'
Pdss2	'01C001C'
Pgbd1	'01C001C'
Pkd2l1	'01C001C'
Ppm1l	'01C001C'
Psmb2	'01C001C'
Rbm24	'01C001C'
Ric8b	'01C001C'
Rnmtl1	'01C001C'
Ropn1l	'01C001C'
Rundc1	'01C001C'
Sdsl	'01C001C'
Siva1	'01C001C'
Slc24a1	'01C001C'
Slc25a40	'01C001C'
Slc38a3	'01C001C'
Smarcd3	'01C001C'
Smpd1	'01C001C'
St3gal3	'01C001C'
Stard10	'01C001C'
Tmem147	'01C001C'
Trak1	'01C001C'
Urod	'01C001C'
Vps4a	'01C001C'
Wdr74	'01C001C'
Zfp212	'01C001C'
Zfp612	'01C001C'
4930504O13Rik	'01D000'
4933406J08Rik	'01D000'

9930032O22Rik	'01D000'
Abcc5	'01D000'
Bad	'01D000'
Cybasc3	'01D000'
D1Pas1	'01D000'
ENSMUSG00000055419	'01D000'
Fgfbp3	'01D000'
Gpr133	'01D000'
Hspb1	'01D000'
Klk10	'01D000'
Rftn2	'01D000'
Xpot	'01D000'
1700057K13Rik	'01D001D'
1700091H14Rik	'01D001D'
2310011E23Rik	'01D001D'
2410024F20Rik	'01D001D'
4922505E12Rik	'01D001D'
4930453O03Rik	'01D001D'
4930513L20Rik	'01D001D'
4930520O04Rik	'01D001D'
4930556N09Rik	'01D001D'
4930557B21Rik	'01D001D'
5430416N02Rik	'01D001D'
6230424C14Rik	'01D001D'
6720482G16Rik	'01D001D'
9030409K20Rik	'01D001D'
9130204L05Rik	'01D001D'
9430098F02Rik	'01D001D'
Alg2	'01D001D'
Ankrd13d	'01D001D'
Ankrd45	'01D001D'
Apobec3	'01D001D'
AU015247	'01D001D'
B130024G19Rik	'01D001D'
B3gnt2	'01D001D'
BC007180	'01D001D'
C630001G18Rik	'01D001D'
C76872	'01D001D'
Crebzf	'01D001D'
Cyp4f41-ps	'01D001D'
D630042F21Rik	'01D001D'
D8Ertd51e	'01D001D'
Defb7	'01D001D'
Dgkz	'01D001D'
Dnase2b	'01D001D'
Efnb2	'01D001D'
EG215714	'01D001D'
Fance	'01D001D'
Fbxl20	'01D001D'
Frem1	'01D001D'

Gnat1	'01D001D'
H60a	'01D001D'
Il31	'01D001D'
Ing2	'01D001D'
Kiss1r	'01D001D'
Lamb1-1	'01D001D'
LOC100048168 /// Sav1	'01D001D'
LOC676708	'01D001D'
Lrrc8d	'01D001D'
Mep1b	'01D001D'
Myo1f	'01D001D'
Olfr157	'01D001D'
OTTMUSG00000018358	'01D001D'
Phex	'01D001D'
Phgdh	'01D001D'
Prelid1	'01D001D'
Psg17	'01D001D'
Rbm31y	'01D001D'
Slc5a4a	'01D001D'
Speer7-ps1 /// Speer8-ps1	'01D001D'
Tnk2	'01D001D'
Unc5b	'01D001D'
Zfp36l1	'01D001D'
Zfp59	'01D001D'
100042529 /// Lgi1	'1A0000'
1110012N22Rik	'1A0000'
1110054M08Rik	'1A0000'
1600014C10Rik	'1A0000'
2010305A19Rik	'1A0000'
2310026E23Rik	'1A0000'
2310040A07Rik	'1A0000'
2410022L05Rik	'1A0000'
2410166I05Rik	'1A0000'
2610036D13Rik	'1A0000'
2900009J06Rik	'1A0000'
5830417C01Rik	'1A0000'
6330578E17Rik	'1A0000'
A130092J06Rik	'1A0000'
A230067G21Rik	'1A0000'
A230083H22Rik	'1A0000'
Abcb6	'1A0000'
Abhd5	'1A0000'
Abhd6	'1A0000'
Acadm	'1A0000'
Acads	'1A0000'
Acsl6	'1A0000'
Acsm5	'1A0000'
Ak3l1 /// LOC100047616 /// OTTMUSG00000013175	'1A0000'
Akap1	'1A0000'
Als2cr2	'1A0000'

Amot	'1A0000'
Amy1	'1A0000'
Ank	'1A0000'
Ankrd40	'1A0000'
Ankrd50	'1A0000'
Apba3	'1A0000'
Asb12	'1A0000'
Atp6v0a2	'1A0000'
Auts2	'1A0000'
BC004004	'1A0000'
Cand2	'1A0000'
Casq1	'1A0000'
Cdc34 /// LOC100046898	'1A0000'
Cdh22 /// LOC100046008	'1A0000'
Clasp1	'1A0000'
Commd9	'1A0000'
Coq3	'1A0000'
Crhr2	'1A0000'
Crip2	'1A0000'
Crybb1	'1A0000'
Csdc2	'1A0000'
Ctf1	'1A0000'
D930015E06Rik	'1A0000'
Dbi	'1A0000'
Dcakd	'1A0000'
Dcun1d4	'1A0000'
Derl2	'1A0000'
Dmpk	'1A0000'
Dnajb4	'1A0000'
Dpyd	'1A0000'
Dusp7	'1A0000'
Egf	'1A0000'
Ehbp1	'1A0000'
Eif2b1	'1A0000'
Enpep	'1A0000'
Entpd5	'1A0000'
Epn3	'1A0000'
Fabp3	'1A0000'
Fads3	'1A0000'
Fbxl17	'1A0000'
Frap1	'1A0000'
Fsd2	'1A0000'
G6pc3	'1A0000'
Gabrg3	'1A0000'
Garnl4	'1A0000'
Gfm1	'1A0000'
Gga2	'1A0000'
Glrx	'1A0000'
Gm944	'1A0000'
Gpsn2	'1A0000'

Grb10	'1A0000'
Grb14	'1A0000'
Grb2	'1A0000'
Gsta1 /// Gsta2 /// LOC100042295	'1A0000'
Hdhd3	'1A0000'
Hspb2	'1A0000'
Hspb3	'1A0000'
Hspb8	'1A0000'
Hspd1	'1A0000'
Igsf1	'1A0000'
Iqgap2	'1A0000'
Iqwd1	'1A0000'
Itgb1bp2	'1A0000'
Kcng2	'1A0000'
Kcnj3	'1A0000'
Klhl30	'1A0000'
Klk1b22 /// Klk1b9	'1A0000'
Kremen1	'1A0000'
Ky	'1A0000'
Lactb /// LOC677144	'1A0000'
Lbh	'1A0000'
Ldb3	'1A0000'
Letm1	'1A0000'
Lgi1	'1A0000'
LOC676546 /// Mmd	'1A0000'
LOC677317 /// Me1	'1A0000'
Lpin1	'1A0000'
Lrrc20	'1A0000'
Lycat	'1A0000'
Magi3	'1A0000'
Mal	'1A0000'
Mapk10	'1A0000'
Mapre3	'1A0000'
Masp1	'1A0000'
Mgmt	'1A0000'
Mlxip	'1A0000'
Morn4	'1A0000'
Mpdz	'1A0000'
Mpi	'1A0000'
Mrpl28	'1A0000'
Mrpl44	'1A0000'
Mrps34	'1A0000'
Mrps6	'1A0000'
Msra	'1A0000'
Mtus1	'1A0000'
Mybpc2	'1A0000'
Myo5b	'1A0000'
Neurl2	'1A0000'
Nkiras1	'1A0000'
Nlrx1	'1A0000'

Nova1	'1A0000'
Nqo1	'1A0000'
Nudt12	'1A0000'
Nudt4	'1A0000'
Nupl2	'1A0000'
Oma1	'1A0000'
Oplah	'1A0000'
Osbpl1a	'1A0000'
Osbpl6	'1A0000'
P2ry2	'1A0000'
P4ha2	'1A0000'
Palb2	'1A0000'
Pdlim7	'1A0000'
Pex11a	'1A0000'
Pex19	'1A0000'
Phkb	'1A0000'
Phtf2	'1A0000'
Pkia	'1A0000'
Pla2g4e	'1A0000'
Pla2g5	'1A0000'
Pm20d1	'1A0000'
Pnpla8	'1A0000'
Polrmt	'1A0000'
Ppapdc3	'1A0000'
Prdx6	'1A0000'
Prkrir	'1A0000'
Prlr	'1A0000'
Psma4	'1A0000'
Rad17	'1A0000'
Raf1	'1A0000'
Rgma	'1A0000'
Rnf10	'1A0000'
Rnf11	'1A0000'
Rnf123	'1A0000'
Rnf5	'1A0000'
Rras2	'1A0000'
Rxrg	'1A0000'
Sacs	'1A0000'
Sardh	'1A0000'
Satb1	'1A0000'
Scube2	'1A0000'
Sema3c	'1A0000'
Setmar	'1A0000'
Sh3gl2	'1A0000'
Sh3rf2	'1A0000'
Slc22a3	'1A0000'
Slc25a20	'1A0000'
Slc25a26	'1A0000'
Slc25a42	'1A0000'
Slc36a2	'1A0000'

Slc37a4	'1A0000'
Smap2	'1A0000'
Spna1	'1A0000'
St3gal5	'1A0000'
Stom	'1A0000'
Suox	'1A0000'
Synj2	'1A0000'
Synpo2	'1A0000'
Timm22	'1A0000'
Tmem141	'1A0000'
Tmem38b	'1A0000'
Tmem53	'1A0000'
Tpst2	'1A0000'
Trim7	'1A0000'
Tsc22d4	'1A0000'
Txndc13	'1A0000'
Ube2h	'1A0000'
Ube2r2	'1A0000'
Wdr20a	'1A0000'
Wwp1	'1A0000'
Xpnpep1	'1A0000'
Xpo4	'1A0000'
2310022A10Rik	'1A001A0'
2400001E08Rik /// EG433216	'1A001A0'
2900046G09Rik	'1A001A0'
4833439L19Rik	'1A001A0'
9030418K01Rik	'1A001A0'
Ahsa2	'1A001A0'
Alpk2	'1A001A0'
Ankrd23	'1A001A0'
Arhgef7	'1A001A0'
B230337E12Rik	'1A001A0'
BC062109	'1A001A0'
Brca2	'1A001A0'
Camk2g /// LOC100045547	'1A001A0'
Cat	'1A001A0'
Cd151	'1A001A0'
Cds1	'1A001A0'
Comt1	'1A001A0'
Cryab	'1A001A0'
Dag1	'1A001A0'
Ddah1	'1A001A0'
Dtx2	'1A001A0'
E130311K13Rik	'1A001A0'
Egln3	'1A001A0'
Erlin2	'1A001A0'
Fahd1	'1A001A0'
Flnc	'1A001A0'
Gnao1	'1A001A0'
Grit	'1A001A0'

Hfe2	'1A001A0'
Hisppd2a	'1A001A0'
Hspb6	'1A001A0'
Htatip2	'1A001A0'
Josd2	'1A001A0'
Lmcd1	'1A001A0'
LOC674712 /// Ptdss1	'1A001A0'
Loh12cr1	'1A001A0'
Lynx1	'1A001A0'
Mad1l1	'1A001A0'
Map1lc3a	'1A001A0'
Mettl9	'1A001A0'
Mllt11	'1A001A0'
Nkain1	'1A001A0'
Nr2f6	'1A001A0'
Nudt18	'1A001A0'
Palmd	'1A001A0'
Park7	'1A001A0'
Pcnx	'1A001A0'
Rab4a	'1A001A0'
Rock2	'1A001A0'
Setd7	'1A001A0'
Slc17a7	'1A001A0'
Slc45a4	'1A001A0'
Smcr7	'1A001A0'
Srl	'1A001A0'
Srxn1	'1A001A0'
Strn3	'1A001A0'
Suds3	'1A001A0'
Tmed8	'1A001A0'
Trim35	'1A001A0'
Ttc7b	'1A001A0'
Ube2d1	'1A001A0'
Usp10	'1A001A0'
Usp45	'1A001A0'
Wfs1	'1A001A0'
Wrb	'1A001A0'
Zscan20	'1A001C0'
Adi1	'1A1A100'
Adra1b	'1A1A100'
Aox1	'1A1A100'
Atf7ip	'1A1A100'
Capn3	'1A1A100'
Chac2	'1A1A100'
Clu	'1A1A100'
Creg1	'1A1A100'
Creg1 /// Pappa2	'1A1A100'
Dbh	'1A1A100'
Dnaic1	'1A1A100'
Itgb6	'1A1A100'

Kbtbd10	'1A1A100'
Kcnk1	'1A1A100'
Krt222	'1A1A100'
Lrtm1	'1A1A100'
Mboat2	'1A1A100'
Mrgprh	'1A1A100'
Mrps12	'1A1A100'
Myl1	'1A1A100'
Ociad2	'1A1A100'
Pisd	'1A1A100'
Ppp1r3d	'1A1A100'
Pstk	'1A1A100'
Rab40b	'1A1A100'
Sar1b	'1A1A100'
Scn4b	'1A1A100'
Slc47a1	'1A1A100'
Thrsp	'1A1A100'
Tmprss4	'1A1A100'
1110034G24Rik	'1B0000'
1700012D01Rik	'1B0000'
1810027O10Rik	'1B0000'
2010002M12Rik	'1B0000'
2310043N10Rik	'1B0000'
2410005O16Rik	'1B0000'
2700060E02Rik	'1B0000'
4933406E20Rik	'1B0000'
9830115L13Rik /// Zc3hav1	'1B0000'
A530016L24Rik	'1B0000'
Acbd4	'1B0000'
Ak2 /// LOC100047005	'1B0000'
Ap4s1	'1B0000'
Arhgap9	'1B0000'
Armcx3 /// LOC100044266	'1B0000'
Bcnp1	'1B0000'
Btg3 /// EG654432 /// LOC100048453	'1B0000'
Camk2n1	'1B0000'
Card10	'1B0000'
Ccbl2	'1B0000'
Cdkl1	'1B0000'
Cetn3	'1B0000'
Chchd3	'1B0000'
Cnksr1	'1B0000'
Cnksr3	'1B0000'
Cox17	'1B0000'
D10Wsu52e	'1B0000'
Ddx1	'1B0000'
Dnajb6	'1B0000'
Doc2g	'1B0000'
Ebp	'1B0000'
Ehd4	'1B0000'

Eif2a	'1B0000'
Eif4ebp1	'1B0000'
ENSMUSG00000072940 /// Rps28	'1B0000'
Exoc6	'1B0000'
Ezh1	'1B0000'
Fgf13	'1B0000'
Fnip2	'1B0000'
Gabarap	'1B0000'
Gcat	'1B0000'
Gcnt1	'1B0000'
Ggnbp2	'1B0000'
Gnb2l1	'1B0000'
Gnb3	'1B0000'
H47	'1B0000'
Hint2	'1B0000'
Hsd17b10	'1B0000'
Igfbp3	'1B0000'
Imp3	'1B0000'
Isyna1	'1B0000'
Klhl13	'1B0000'
Lamb3	'1B0000'
Las1l	'1B0000'
Lmo2 /// LOC100048263	'1B0000'
LOC100044627 /// Rpl23	'1B0000'
LOC100045332 /// LOC636901 /// Rpsa	'1B0000'
LOC100047324 /// Sesn1	'1B0000'
Mamdc2	'1B0000'
Mrps24	'1B0000'
Mylk3	'1B0000'
Obscn	'1B0000'
OTTMUSG00000016200 /// OTTMUSG00000022847 /// Rps8	'1B0000'
OTTMUSG00000016644	'1B0000'
Perp	'1B0000'
Phc3	'1B0000'
Pold2	'1B0000'
Polr2g	'1B0000'
Ppp1ca	'1B0000'
Prps2	'1B0000'
Psmc3	'1B0000'
Ptpn14	'1B0000'
Pygl	'1B0000'
Rarres2	'1B0000'
Rhou	'1B0000'
Rnaseh2b	'1B0000'
Rpl18a	'1B0000'
Rplp1	'1B0000'
Rps17	'1B0000'
Rps3	'1B0000'
Rps4x	'1B0000'
Sepp1	'1B0000'

Serpinb6b	'1B0000'
Shfm1	'1B0000'
Spcs1	'1B0000'
Stk39	'1B0000'
Tcp11l2	'1B0000'
Timp3	'1B0000'
Tmem128	'1B0000'
Tmem71	'1B0000'
Tomm7	'1B0000'
Tpd52l1	'1B0000'
Trappc6a	'1B0000'
Ung	'1B0000'
Vamp5	'1B0000'
Wipf3	'1B0000'
Xbp1	'1B0000'
Xpo1	'1B0000'
Ypel3	'1B0000'
Zfp187	'1B0000'
Zfp383	'1B0000'
Zfyve21	'1B0000'
Zmym5	'1B0000'
Mosc2	'1B001A0'
100038991 /// 100043296 /// ENSMUSG00000069439 /// Rpl35	'1B001B0'
100038991 /// Rpl35	'1B001B0'
100040123 /// EG383032 /// EG665772 /// LOC674335 /// Rps17	'1B001B0'
100040123 /// Rps17	'1B001B0'
100041163 /// 100041478 /// ENSMUSG00000063556 /// LOC100046821 /// Rpl23a	'1B001B0'
100041237 /// Nudc /// Nudc-ps1	'1B001B0'
100041294 /// Supt4h1	'1B001B0'
100042986 /// 668941 /// Rpl37a	'1B001B0'
100043039 /// ENSMUSG00000066757 /// OTTMUSG00000002238 /// Sec61g	'1B001B0'
100043481 /// OTTMUSG00000009529 /// Rpl37	'1B001B0'
100043718 /// LOC100048508 /// OTTMUSG00000012957 /// Rpl36	'1B001B0'
1600020E01Rik	'1B001B0'
2310005N03Rik	'1B001B0'
2310016C16Rik	'1B001B0'
2310016E02Rik	'1B001B0'
2810004N23Rik /// Setd6	'1B001B0'
2900010J23Rik	'1B001B0'
677010 /// EG667779 /// OTTMUSG00000005566 /// Rpl30	'1B001B0'
Acbd7	'1B001B0'
Adcy6	'1B001B0'
Aldh7a1	'1B001B0'
Anapc11	'1B001B0'
Anapc13	'1B001B0'
Ankrd29	'1B001B0'
Asb11	'1B001B0'
BC023892	'1B001B0'
Bloc1s1	'1B001B0'
Brcc3	'1B001B0'

Ccdc5	'1B001B0'
Ccrl2	'1B001B0'
Cdc123	'1B001B0'
Cryzl1	'1B001B0'
Ctnnal1	'1B001B0'
D630004K10Rik	'1B001B0'
Dcxr	'1B001B0'
Dhrs7	'1B001B0'
Efcab2	'1B001B0'
EG621100 /// OTTMUSG00000001643 /// Rpl27	'1B001B0'
EG625298 /// ENSMUSG00000066362 /// LOC100044992 /// LOC100048340 /// Rps13	'1B001B0'
EG627737 /// mCG_130059 /// Rpl22	'1B001B0'
EG629116 /// EG668041 /// LOC677113 /// Rps24	'1B001B0'
EG629116 /// LOC677113 /// Rps24	'1B001B0'
EG640050 /// Rps7	'1B001B0'
EG668144 /// ENSMUSG00000062611 /// Rps3a	'1B001B0'
Eif3e	'1B001B0'
Eif3k	'1B001B0'
ENSMUSG00000050299 /// Fau	'1B001B0'
ENSMUSG00000059775 /// LOC100047845 /// Rps26	'1B001B0'
ENSMUSG00000069117 /// LOC100047828 /// Rps18	'1B001B0'
Fasn	'1B001B0'
Fbln1	'1B001B0'
Gas5	'1B001B0'
Gchfr	'1B001B0'
Gtf2b	'1B001B0'
Hddc2	'1B001B0'
Hebp1	'1B001B0'
Hint3	'1B001B0'
Igbp1	'1B001B0'
Immp2l	'1B001B0'
Irak1bp1	'1B001B0'
Irf2bp2	'1B001B0'
Jak1	'1B001B0'
Krtcap2	'1B001B0'
LOC100039355 /// Rps16	'1B001B0'
LOC100045856 /// Sunc1	'1B001B0'
LOC100046668 /// OTTMUSG00000022083 /// Rps23	'1B001B0'
LOC100048508 /// OTTMUSG00000012957 /// Rpl36	'1B001B0'
Lsm3	'1B001B0'
Lyar	'1B001B0'
Mecp2	'1B001B0'
Mfap1a /// Mfap1b	'1B001B0'
Mxi1	'1B001B0'
Nenf	'1B001B0'
Nsmce4a	'1B001B0'
OTTMUSG00000004411 /// Uba52	'1B001B0'
OTTMUSG00000007332	'1B001B0'
OTTMUSG00000022086 /// Rpl10a	'1B001B0'
OTTMUSG00000022843 /// Rpl5	'1B001B0'

Pcbd2	'1B001B0'
Pdcd5	'1B001B0'
Pfdn5	'1B001B0'
Pigf	'1B001B0'
Pigp	'1B001B0'
Polb	'1B001B0'
Polr2e	'1B001B0'
Ppp1r11	'1B001B0'
Rabac1	'1B001B0'
Rbp4	'1B001B0'
Rdm1	'1B001B0'
Retn	'1B001B0'
Rit1	'1B001B0'
Rnf114	'1B001B0'
Rpl11	'1B001B0'
Rpl12	'1B001B0'
Rpl18	'1B001B0'
Rpl23	'1B001B0'
Rpl7	'1B001B0'
Rplp0	'1B001B0'
Rps15	'1B001B0'
Rps21	'1B001B0'
Rps25	'1B001B0'
Rps27	'1B001B0'
Rps5	'1B001B0'
Rps7	'1B001B0'
Rps9	'1B001B0'
Selk	'1B001B0'
Smoc2	'1B001B0'
Smpdl3a	'1B001B0'
Snrpe	'1B001B0'
Spa17	'1B001B0'
Stag2	'1B001B0'
Stxbp6	'1B001B0'
Them2	'1B001B0'
Tinagl1	'1B001B0'
Tlcd1	'1B001B0'
Tusc3	'1B001B0'
Txndc16	'1B001B0'
Wrnip1	'1B001B0'
1700025G04Rik	'1B1B100'
2310056P07Rik	'1B1B100'
Abcg2	'1B1B100'
Akt1 /// LOC100047666	'1B1B100'
Atpif1	'1B1B100'
Bex1	'1B1B100'
Ccni	'1B1B100'
Cobl	'1B1B100'
Dusp4	'1B1B100'
Ednra	'1B1B100'

Hrasls3	'1B1B100'
Igf1r	'1B1B100'
Irs1	'1B1B100'
Klhdc2	'1B1B100'
LOC100045031 /// Tceal8	'1B1B100'
LOC672215 /// Ntn1	'1B1B100'
Mak10	'1B1B100'
Myom2	'1B1B100'
Plcd3	'1B1B100'
S100a13	'1B1B100'
Tfpi	'1B1B100'
Tmem100	'1B1B100'
Tmem120a	'1B1B100'
Tmem164	'1B1B100'
Dnajc4	'1B1C100'
Mrpl23 /// OTTMUSG00000013301	'1B1C100'
2900011O08Rik	'1C0000'
3200001D21Rik	'1C0000'
As3mt	'1C0000'
Btbd11	'1C0000'
C79557	'1C0000'
D330028D13Rik	'1C0000'
Dleu2	'1C0000'
EG226957	'1C0000'
Gpr137c	'1C0000'
Lrrtm4	'1C0000'
Mtrf1l	'1C0000'
Qsox2	'1C0000'
Tyrp1	'1C0000'
328235	'1C001C0'
1300002E11Rik	'1C001C0'
1500004A13Rik	'1C001C0'
1700021P04Rik	'1C001C0'
1700061J05Rik	'1C001C0'
1700074P13Rik	'1C001C0'
1700105P06Rik	'1C001C0'
2510049J12Rik	'1C001C0'
2700049P18Rik	'1C001C0'
4921525D07Rik	'1C001C0'
4930466I24Rik	'1C001C0'
4930521A18Rik	'1C001C0'
4930563P21Rik	'1C001C0'
4931423N10Rik	'1C001C0'
4933431M02Rik	'1C001C0'
6030419C18Rik	'1C001C0'
6230400D17Rik	'1C001C0'
6330408A02Rik	'1C001C0'
9030420N05Rik	'1C001C0'
9330199C07Rik	'1C001C0'
A430088P11Rik	'1C001C0'

A930003G23Rik	'1C001C0'
AI448005	'1C001C0'
AI480526	'1C001C0'
Akap10	'1C001C0'
Aldob	'1C001C0'
C79468	'1C001C0'
C80719	'1C001C0'
C86544	'1C001C0'
Cdx4	'1C001C0'
Chd6	'1C001C0'
D13Ertd212e	'1C001C0'
D4Ertd199e	'1C001C0'
D5Ertd159e	'1C001C0'
Dalrd3 /// Wdr6	'1C001C0'
Dleu7	'1C001C0'
Dsc1	'1C001C0'
EG545216 /// Glcci1 /// LOC100046012	'1C001C0'
Fabp9	'1C001C0'
Fbxl19	'1C001C0'
Gabra1	'1C001C0'
Gc	'1C001C0'
Gfap	'1C001C0'
Gm527	'1C001C0'
Gsdmc2 /// LOC100045250	'1C001C0'
Gsg1	'1C001C0'
Hivep3 /// LOC100045240	'1C001C0'
Kif4	'1C001C0'
Krtap11-1	'1C001C0'
Krtap16-5	'1C001C0'
Lce1d	'1C001C0'
Lcorl	'1C001C0'
LOC100047468 /// Nxnl1	'1C001C0'
Muc13	'1C001C0'
Myo5c	'1C001C0'
Nmu	'1C001C0'
Npas4	'1C001C0'
Olfr658	'1C001C0'
Pabpnl1	'1C001C0'
Pou2f3	'1C001C0'
Ptprt	'1C001C0'
Rel	'1C001C0'
RP23-394O9.3	'1C001C0'
Serpina12	'1C001C0'
Slc6a13	'1C001C0'
Slfnl1	'1C001C0'
Syt6	'1C001C0'
Tbx6	'1C001C0'
Tmem151a	'1C001C0'
Trhr	'1C001C0'
Tssk2	'1C001C0'

Tyr	'1C001C0'
Upb1	'1C001C0'
V1ra5	'1C001C0'
Zcchc13	'1C001C0'
Slc39a2	'1C1C100'
4932431H17Rik	'1C1D100'
D1Ertd646e	'1C1D100'
668215	'1D0000'
4833412C15Rik	'1D0000'
4930428B01Rik	'1D0000'
9230102K24Rik	'1D0000'
AI465300	'1D0000'
AI646023	'1D0000'
C730048C13Rik	'1D0000'
Cyb561d1	'1D0000'
Dars	'1D0000'
Degs1	'1D0000'
Derl1	'1D0000'
EG622268 /// Mrpl27	'1D0000'
Gadd45b	'1D0000'
LOC100044475 /// Nck2	'1D0000'
LOC433466 /// Pla2g4b	'1D0000'
Nr2c2	'1D0000'
Nup98	'1D0000'
Ptrh2	'1D0000'
Rer1	'1D0000'
Sdhd	'1D0000'
Sema5a	'1D0000'
100042741 /// LOC100046556 /// Zfp706	'1D001D0'
1700113I22Rik	'1D001D0'
1810058N15Rik	'1D001D0'
2210011K15Rik	'1D001D0'
2310061A09Rik	'1D001D0'
4933416C03Rik	'1D001D0'
5730405A17Rik	'1D001D0'
671392 /// LOC100047898 /// Set	'1D001D0'
6720457D02Rik	'1D001D0'
A630035D09Rik	'1D001D0'
AI848100	'1D001D0'
Akr1c12	'1D001D0'
Apol7a	'1D001D0'
Atp13a3	'1D001D0'
Atp8b2	'1D001D0'
B3galt4	'1D001D0'
BC031748	'1D001D0'
Bmper	'1D001D0'
Cep120	'1D001D0'
Crip3	'1D001D0'
Cxcl1	'1D001D0'
Cyfip1	'1D001D0'

D130062J10Rik	'1D001D0'
D6Ertd527e	'1D001D0'
D7Ertd1e	'1D001D0'
Dnm2	'1D001D0'
Dync1i2	'1D001D0'
ENSMUSG00000053185	'1D001D0'
Evpl	'1D001D0'
F11	'1D001D0'
Gria4	'1D001D0'
Hmga1 /// Hmga1-rs1	'1D001D0'
Klf11	'1D001D0'
Klrg1	'1D001D0'
LOC100044385	'1D001D0'
LOC100045432 /// Stim1	'1D001D0'
LOC541456	'1D001D0'
Med15	'1D001D0'
Mobkl2b	'1D001D0'
Mppe1	'1D001D0'
Pgm3	'1D001D0'
Pnlip	'1D001D0'
Pnpo	'1D001D0'
Prl7c1	'1D001D0'
Rage	'1D001D0'
Rbm15	'1D001D0'
Rcl1	'1D001D0'
Rcor3	'1D001D0'
Rhbdd1	'1D001D0'
Rmnd5b	'1D001D0'
Rnasel	'1D001D0'
Rpa1	'1D001D0'
Sdk1	'1D001D0'
Selp	'1D001D0'
Spats2	'1D001D0'
Sptlc1	'1D001D0'
Tax1bp1	'1D001D0'
Tfip11	'1D001D0'
Tjp2	'1D001D0'
Tmem67	'1D001D0'
Treh	'1D001D0'
Vsx1	'1D001D0'
Wdr25	'1D001D0'
Wdr33	'1D001D0'
Zzz3	'1D001D0'
Tmem179b	'1D1D100'

Phosphoinositide 3-Kinase (PI3K(p110α)) Directly Regulates Key Components of the Z-disc and Cardiac Structure

Ashley J. Waardenberg, Bianca C. Bernardo, Dominic C. H. Ng, Peter R. Shepherd, Nelly Cemerlang, Mauro Sbroggiò, Christine A. Wells, Brian P. Dalrymple, Mara Brancaccio, Ruby C. Y. Lin and Julie R. McMullen

J. Biol. Chem. 2011, 286:30837-30846.
doi: 10.1074/jbc.M111.271684 originally published online July 11, 2011
